Department of Chemical and Metallurgical Engineering

Phase equilibria and precious or high-tech metal distributions in copper smelting systems

Min Chen

Aalto University

DOCTORAL THESES

Aalto University publication series
DOCTORAL THESES 146/2022

Phase equilibria and precious or high-tech metal distributions in copper smelting systems

Min Chen

A doctoral thesis completed for the degree of Doctor of Science (Technology) to be defended, with the permission of the Aalto University School of Chemical Engineering, at a public examination held at the lecture hall Ke2 of the school on 28 October 2022 at 12 o'clock.

Aalto University
School of Chemical Engineering
Department of Chemical and Metallurgical Engineering
Metallurgy

Supervising professor
Professor Ari Jokilaakso, Aalto University, Finland

Thesis advisors
D.Sc. (Tech.) Katri Avarmaa, Aalto University, Finland
Professor Emeritus Pekka Taskinen, Aalto University, Finland

Preliminary examiners
Professor Tianzu Yang, Central South University, China
Professor Bogusław Zbigniew Onderka, AGH University of Science and Technology, Poland

Opponent
D.Sc. (Tech.) Taufiq Hidayat, Bandung Institute of Technology, Indonesia

Aalto University publication series
DOCTORAL THESES 146/2022

ISBN 978-952-64-0973-3 (printed)
ISBN 978-952-64-0974-0 (pdf)
ISSN 1799-4934 (printed)
ISSN 1799-4942 (pdf)
http://urn.fi/URN:ISBN:978-952-64-0974-0

Images: Min Chen

Unigrafia Oy
Helsinki 2022

Finland

NORDIC SWAN ECOLABEL
Printed matter
4041-0619

Author
Min Chen

Name of the doctoral thesis
Phase equilibria and precious or high-tech metal distributions in copper smelting systems

Publisher School of Chemical Engineering

Unit Department of Chemical and Metallurgical Engineering

Series Aalto University publication series DOCTORAL THESES 146/2022

Field of research Processing of Materials

Manuscript submitted 2 September 2022 **Date of the defence** 28 October 2022

Permission for public defence granted (date) 21 September 2022 **Language** English

☐ **Monograph** ☒ **Article thesis** ☐ **Essay thesis**

Abstract

Metals have historically played an important role in modern societies and the industrial revolution. Nowadays, however, they are mainly derived from primary ore resources and secondary materials, such as waste electrical and electronic equipment (WEEE). WEEE contains a variety of products that no longer serve their initial purpose and their metal concentrations are significantly higher than that in primary ores. In the face of a strong demand for a circular economy model, the recovery of metal values from WEEE has attracted increasing attention. Base metals like copper, lead, and nickel are good collector metals for precious/high-tech metals. Therefore, the smelting technologies of base metals are potential and effective methods for recycling metals from secondary materials. To have a better understanding of the favorable conditions for the recoveries of valuable metals from secondary materials through copper smelting, it is critical to determine the behavior of various metals in copper smelting systems.

In this study, the phase equilibria of matte/copper and silica/spinel/wüstite-saturated iron silicate slags as well as the distribution equilibria of precious (Au, Ag, Pt, and Pd) and high-tech (Ni, Co, and Sn) metals in the equilibrium systems were investigated using an advanced high-temperature isothermal equilibration/quenching technique, followed by direct phase composition analyses using electron probe X-ray microanalysis (EPMA) and laser ablation-inductively coupled plasma-mass spectrometry (LA-ICP-MS). The experimental parameters and conditions were selected to simulate primary and secondary copper smelting processes. An investigation was made of the effects of pSO_2, the slag modifiers Al_2O_3 and CaO, the temperature, and the saturation phase on the equilibrium phase relations of copper/matte and slag, as well as on the equilibrium distributions of the aforementioned precious/high-tech metals.

The equilibrium compositions of matte/metal, slag, and spinel/wüstite were displayed as a function of matte grade or oxygen partial pressure. The distribution coefficients of precious/high-tech metals between matte/metal and spinel/wüstite/slag were calculated based on experimentally determined metal concentrations in matte, slag, and spinel/wüstite. The novel experimental data obtained in this study provide insights for improving the performance of copper smelters and increasing the recovery of valuable metals from primary and secondary materials by adjusting the temperature and oxygen partial pressure, and by adding fluxes like Al_2O_3 and CaO. Moreover, the present results are useful for thermodynamic database development and for the modeling of the phase relations of major components and precious/high-tech metals distributions in copper smelting systems.

Keywords resource efficiency, circular economy, waste management, recycling, secondary materials

ISBN (printed) 978-952-64-0973-3 **ISBN (pdf)** 978-952-64-0974-0

ISSN (printed) 1799-4934 **ISSN (pdf)** 1799-4942

Location of publisher Helsinki **Location of printing** Helsinki **Year** 2022

Pages 170 **urn** http://urn.fi/URN:ISBN:978-952-64-0974-0

Preface

The joy of receiving the admission letter for the doctoral study program seems like only yesterday, but the life of my doctoral research is about to end. The research experience in Finland will be one of the most unforgettable memories of my whole life, which cultivated my ability to identify and get over scientific obstacles. The research work presented in this doctoral thesis was carried out at Aalto University, School of Chemical Engineering, Department of Chemical and Metallurgical Engineering, and the Metallurgy research group (MTG). The research work in the MTG group started in December 2018 with financial support from the China Scholarship Council (grant number 201806370217) and the Business Finland funded SYMMET project (grant number 3891/31/2018).

First of all, I want to express my deep gratitude to my supervisor, Professor Ari Jokilaakso. Thank you for providing me with the opportunity to study in Finland after I graduated from Central South University. You have given me much respect, support, and freedom to do the research that I am interested in. At the same time, I greatly appreciate your care and respect for me. Great thanks also go to my thesis advisor, Professor emeritus Pekka Taskinen. Thanks for your guidance in making the experimental design of my research, your instructions for writing, and your valuable comments in the early mornings. Your careful attitude toward academic research and your rich knowledge of pyrometallurgy have affected me in a profound way.

I would also like to express sincere appreciation to my thesis instructor, Dr. Katri Avarmaa. I cannot imagine how hard my life would be without your encouragement during my studies and your instructions on solving the problems encountered during my research. Thanks also to Dr. Lassi Klemettinen who taught me multiple experimental skills and guided me on how to survive in the pyrometallurgy lab. Special thanks go to Dr. Junjie Shi for your instructions on doing phase diagram research, which helped me to have a better understanding of pyrometallurgical processes. Thank you, Dr. Hugh O'Brien and Dr. Radoslaw Michallik, for your assistance in EPMA and LA-ICP-MS analyses. I am also grateful to Professor Daniel Lindberg for your patience in teaching me thermodynamic calculations using FactSage. My current and former colleagues in Aalto: Dmitry Sukhomlinov, Imam Santoso, Min-kyu Paek, Anna Klemettinen, Yun Li, Leiting Shen, Xingbang Wan, Chao Peng, Fupeng Liu, Fang Hu, Zulin Wang, Jianxin Zhang, Kezhou Song, Yuanmin Zou, Minna Rämä, David Sibarani, Junmo Jeon, Ronja Ruismäki, Yujie Chen, Miao Tian and all the others, are acknowledged for your great support and valuable discussions. I value the friendship with our "Fisherman" teammates: Haoran Sun, Chao Yang, Sinan Lin, and Xiaobo Wu.

Last but not least, my deepest thanks go to my parents, my sister, and my brother-in-law. Thank you for your selfless sacrifice, encouragement, and inspiration. The journey to chase my dream would have been much more difficult without your support.

JMT 1, Espoo
08 April 2022
Min Chen

Contents

List of Abbreviations and Symbols

Abbreviations

AES	Atomic emission spectrometry
BMO	Base Metals Operation
BSE	Backscattered electron
CA	Chemical analysis
EDS	Energy dispersive spectrometry
EF	Electric smelting furnace
EPMA	Electron probe X-ray microanalysis
FSF	Flash smelting furnace
GTK	Geological Survey of Finland
ICP	Inductively coupled plasma
LA-ICP-MS	Laser ablation-inductively coupled plasma-mass spectrometry
Me	Metal
MTG	Metallurgy research group at Aalto University
NIST	National Institute of Standards and Technology (USA)
PAP	Pouchou and Pichoir matrix correction model
PGMs	Platinum group metals
PMO	Precious Metals Operation
PMs	Precious metals
PS	Peirce-Smith
SEM	Scanning electron microscope

TRA	Time-resolved analysis
TSL	Top submerged lance
USGS	United States Geological Survey
WDS	Wavelength dispersive spectrometry
WEEE	Waste electrical and electronic equipment
XRD	X-ray diffraction
ZAF	Atomic number (Z)-absorption (A)-fluorescence (F) matrix correction

Symbols

$a(MeO_v)$	Activity of metal oxide MeO_v
a[Me]	Activity of metal Me
J/cm^2	Joules per square centimeter
K	Equilibrium constant
$L^{Cu/S}$	Distribution coefficient between copper and slag
$L^{m/s}$	Distribution coefficient between matte and slag
$L_{Me}^{A/B}$	Distribution coefficient of Me between phase A and phase B
$L^{Solid/S}$	Distribution coefficient between solid and slag
$L^{Sp/S}$	Distribution coefficient between spinel and slag
$ngTEQ/Nm^3$	Nanogram toxic equivalent quantity per standard cubic meter
n_T	Total mole number of mono-cationic constituents in different phase
pO_2	Oxygen partial pressure (standard state 1 atm)
ppmw	Parts per million by weight
pS_2	Sulfur partial pressure (standard state 1 atm)
pSO_2	Sulfur dioxide partial pressure (standard state 1 atm)
T	Temperature
t	Ton
vol%	Volume percent

wt%	Weight percent
γMe	Activity coefficients of metal Me
γMeO_v	Activity coefficients of metal oxide MeO_v

List of Publications

This doctoral dissertation consists of a summary and of the following publications which are referred to in the text by their numerals.

1. Chen, M., Avarmaa, K., Klemettinen, L., O'Brien, H., Sukhomlinov, D., Shi, J., Taskinen, P., & Jokilaakso, A. (2020). Recovery of precious metals (Au, Ag, Pt, and Pd) from urban mining through copper smelting. *Metallurgical and Materials Transactions B*, 51(4), 1495-1508. https://doi.org/10.1007/s11663-020-01861-5

2. Chen, M., Avarmaa, K., Klemettinen, L., Shi, J., Taskinen, P., Lindberg, D., & Jokilaakso, A. (2020). Equilibrium of copper matte and silica-saturated iron silicate slags at 1300 °C and P_{SO_2} of 0.5 atm. *Metallurgical and Materials Transactions B*, 51(5), 2107-2118. https://doi.org/10.1007/s11663-020-01933-6

3. Chen, M., Avarmaa, K., Klemettinen, L., O'Brien, H., Shi, J., Taskinen, P., Lindberg, D., & Jokilaakso, A. (2021). Precious metal distributions between copper matte and slag at high P_{SO_2} in WEEE reprocessing. *Metallurgical and Materials Transactions B*, 52(2), 871-882. https://doi.org/10.1007/s11663-021-02059-z

4. Chen, M., Avarmaa, K., Taskinen, P., Klemettinen, L., Michallik, R., O'Brien, H., & Jokilaakso, A. (2021). Handling trace elements in WEEE recycling through copper smelting-an experimental and thermodynamic study. *Minerals Engineering*, 173, 107189. https://doi.org/10.1016/j.mineng.2021.107189

5. Chen, M., Avarmaa, K., Taskinen, P., Michallik, R., & Jokilaakso, A. (2022). An experimental study on the phase equilibria of FeOx-saturated iron silicate slags and metallic copper alloys at 1200-1300 °C. *Calphad: Computer Coupling of Phase Diagrams and Thermochemistry*, 77, 102418. https://doi.org/10.1016/j.calphad.2022.102418

6. Chen, M., Avarmaa, K., Taskinen, P., Klemettinen, L., Michallik, R., O'Brien, H., & Jokilaakso, A. (2022). Novel fluxing strategy of copper matte smelting and trace metals in e-waste recycling. Submitted to *Minerals Engineering*, 06/2022.

Author's Contribution

Publication 1: Recovery of precious metals (Au, Ag, Pt, and Pd) from urban mining through copper smelting

M.C. designed the experimental plan instructed by K.A., P.T., and A.J. M.C. conducted the experiments and the analysis of the results. The LA-ICP-MS analyses were conducted by L.K. and H.O. M.C. wrote the first version of the manuscript with valuable input from D.S and J.S. The final draft was prepared in cooperation with all of the authors.

Publication 2: Equilibrium of copper matte and silica-saturated iron silicate slags at 1300 °C and P_{SO_2} of 0.5 atm

M.C. designed the experimental plan together with K.A. and P.T. M.C. executed the experiments and the analysis of the results with assistance from J.S. The LA-ICP-MS analyses were conducted by L.K. and H.O. M.C. prepared the first version of the manuscript, and the final version was reviewed by all of the authors. A.J. and D.L. provided the research funding.

Publication 3: Precious metal distributions between copper matte and slag at high P_{SO_2} in WEEE reprocessing

M.C. designed the experimental plan together with K.A. and P.T. M.C. conducted the experiments and characterized the samples by SEM-EDS with assistance from J.S. L.K. and H.O. offered help for the LA-ICP-MS analyses. M.C wrote the first version of the manuscript, and the final version was prepared with input from all of the authors. A.J. supervised the work and D.L. provided the research funding.

Publication 4: Handling trace elements in WEEE recycling through copper smelting-an experimental and thermodynamic study

M.C. designed the experimental plan in cooperation with K.A. and P.T. M.C. conducted the experiments and carried out the preliminary sample characterizations. R.M. offered valuable help for the EPMA analyses. L.K. and H.O. conducted the LA-ICP-MS analyses. A.J. supervised the work and provided research funding. M.C. prepared the first version of the manuscript, and the final version was reviewed by all of the authors.

Publication 5: An experimental study on the phase equilibria of FeO_x-saturated iron silicate slags and metallic copper alloys at 1200-1300 °C

M.C. designed the experimental plan in cooperation with K.A. and P.T. R.M. gave valuable input to sample characterization by EPMA. A.J. acted as supervisor, provided funding for the

research work, and commenting on the manuscript. P.T. conducted the thermodynamic modeling using MTDATA. M.C. wrote the first version of the manuscript. K.A., P.T., and A.J. reviewed the final version.

Publication 6: Novel fluxing strategy of copper matte smelting and trace metals in e-waste recycling

M.C. designed the experimental plan together with K.A. and P.T. M.C conducted the experiments and interpreted the SEM-EDS and EPMA results. The EPMA analyses were conducted with assistance from R.M. L.K. and H.O. offered valuable help regarding the LA-ICP-MS analyses. A.J. acted as supervisor and provided funding for the research work. M.C wrote the first version of the manuscript and revised the manuscript based on the comments from all of the authors.

1. Introduction

Copper, the third most produced metal in the world, is mainly processed in pyrometallurgical primary and secondary copper smelters [1-3]. Due to the depletion of primary metal resources and tighter environmental protection requirements [4, 5], secondary materials, such as metallurgical wastes and waste electrical and electronic equipment (WEEE), have been introduced into copper smelters as a feedstock [6-13]. Recycling secondary materials has important economic and environmental significance in securing the availability of metals [9, 14, 15].

WEEE contains metallic and non-metallic materials, including plastics, ceramics, common metals (Fe, Cu. Al), precious metals (Au, Ag, Pt, and Pd), heavy metals (Pb, Hg, Cr, and As, etc.), and other high-tech metals (Ni, Co, and Sn) [1, 2, 15-18]. The concentrations of precious and high-tech metals in WEEE vary typically from ppmw to a few percent but many of them are several orders of magnitude higher in WEEE in comparison to their concentrations in natural ores [15, 19-21]. Precious and high-tech metals are widely used by the electronics industry as a hybrid paste to improve the electrical conductivity of joints [22, 23]. Therefore, the main economic value for WEEE recycling currently lies in the recovery of precious and other rare, critical metals.

The copper smelting technologies are regarded as promising methods for recycling valuable metals from secondary materials due to the strong affinities of precious and high-tech metals to metallic copper/copper matte [24-37]. Furthermore, compared with other recycling routes, pyrometallurgical WEEE processing through copper smelting has the advantages of large-scale production, strong adaptability for many types of WEEE, and easy handling of gas emissions and dust without additional investment in an existing plant. Typically, the pyrometallurgical WEEE recycling route starts with collection, dismantling/crushing, and physical separation [38]. Subsequently, the separated copper-rich scraps are fed into primary/secondary copper smelters. During smelting, metals report to different phases, i.e., metal/matte, slag, spinel/wüstite, and a gas stream, depending on their thermodynamic properties [2, 35]. Therefore, the study of the distributions of valuable metals in copper smelting systems under different conditions can provide guidance for improving their recovery from WEEE. Furthermore, the slag volume produced and the concentrations of Al_2O_3, CaO, and MgO in slag are increasing due to the depletion of mineral ores and the addition of secondary materials [39-41]. To improve the performance of copper smelters, it is important to obtain an accurate fundamental thermodynamic phase equilibrium and slag chemistry knowledge of the copper smelting systems.

Over the past few decades, the phase equilibria and trace element distributions have been mainly investigated concerning the FeO_x-SiO_2 slag system and copper or matte at silica/MgO saturation [42-52]. The conventional chemical bulk analysis method for physically separated

phases has been used in most of the previous studies for characterizing the phase compositions. However, the possibly incomplete separation of metal/matte and slag has led to difficulties in deriving accurate results for the phase relations and metal distributions. The direct phase analysis technique electron probe X-ray microanalysis (EPMA) has been used with higher accuracy in phase equilibrium studies to measure phase composition on polished cross-sections of samples. However, the sensitivity of EPMA is still limited and not adequate when determining the concentrations of minor elements in certain phases. To obtain results for minor elements at very low concentrations (on ppmw level) in metallurgical samples, the LA-ICP-MS technique, which has been widely used in the geological sciences, has been used for the first time by researchers from Aalto University [53]. Subsequently, extensive research on trace metal distributions has been carried out using the EPMA and LA-ICP-MS analytical techniques [25-36, 54-68]. Nevertheless, accurate data on many minor/trace elements are still lacking under various conditions (temperature, gas atmosphere, saturation phase, slag composition, etc.) related to different pyrometallurgical copper processes.

1.1 Objective of the thesis

Theoretically, it is possible to recover all valuable metals from secondary materials provided that their distribution mechanism is determined. With the purpose of enriching the experimental thermodynamic data on minor element distributions, the phase equilibria of copper/matte and silica/spinel/wüstite-saturated iron silicate slags, as well as the distribution behaviors of selected precious/high-tech metals (Au, Ag, Pt, Pd, Ni, Co, and Sn) in copper smelting systems, were investigated in this thesis. The precious/high-tech metals were selected due to their high commercial value compared with other minor elements. The conditions were selected to simulate primary and secondary copper smelting processes. The objectives of this thesis are listed based on the timeline of the research:

1. The distribution behaviors of precious metals Au, Ag, Pt, and Pd between copper matte and silica-saturated FeO_x-SiO_2, FeO_x-SiO_2-Al_2O_3, and FeO_x-SiO_2-Al_2O_3-CaO slags at 1300 °C and pSO_2 of 0.1 atm.
2. The distribution behaviors of Au, Ag, Pt, and Pd between copper matte and silica-saturated FeO_x-SiO_2, FeO_x-SiO_2-Al_2O_3, FeO_x-SiO_2-Al_2O_3-CaO slags at high pSO_2.
3. The distributions of Ag, Ni, Co, and Sn between copper alloy and spinel/wüstite-saturated FeO_x-SiO_2 slag related to secondary copper smelting.
4. The distributions of Ag, Ni, Co, and Sn between matte and spinel-saturated FeO_x-SiO_2, FeO_x-SiO_2-Al_2O_3, and FeO_x-SiO_2-CaO slags.
5. The equilibrium phase relations of matte/metal-slag systems.

The matte-slag-tridymite-gas equilibrium experiments were conducted at 1300 °C and a pSO_2 of 0.1-0.5 atm associated with primary copper smelting with air and oxygen-enriched air blowing. The matte-slag-spinel-gas equilibrium experiments were carried out at 1250 °C and a pSO_2 of 0.25 atm. For the copper-slag-spinel/wüstite-gas equilibrium systems, the experimental constraints of 1200-1300 °C and a pO_2 of 10^{-10}-$10^{-6.5}$ atm were selected, which are associated with the secondary copper smelting process. To have a better understanding of the behaviors of trace metals in copper smelting processes, the high-temperature isothermal equilibration/quenching/EPMA/LA-ICP-MS technique was used in this work to determine the distributions of various trace metals in different copper smelting systems corresponding to primary and secondary copper smelting processes.

1.2 New scientific contribution

Accurate fundamental thermodynamic data on the phase equilibria and distributions of trace metals in the metal/matte-slag equilibrium systems measured for the first time are useful for understanding and improving the recoveries of metal values from secondary materials through the current existing copper smelting processes. No studies have previously been carried out on the distributions of Ag, Ni, Co, and Sn between the copper alloy and spinel/wüstite saturated slag, nor on the dissolution of trace metals in solid spinel/wüstite phases, using the quenching/EPMA/LA-ICP-MS technique. Additionally, this is the first study reporting the effects of pSO_2 and the slag modifiers Al_2O_3 and CaO on precious metal distributions between matte and slag. The equilibrium data on matte/copper and slag at spinel/wüstite saturation are very limited. Therefore, the novel phase equilibrium information between copper/matte and silica/spinel/wüstite-saturated iron silicate slags enriches the fundamental experimental thermodynamic data for adjusting the fluxing chemistry and lowering the slag-to-copper ratio in smelting, for example.

1.3 Practical applications

Pyrometallurgical WEEE recycling routes have been adopted in many non-ferrous smelters for recycling valuable metals. Nevertheless, a significant gap in the knowledge of the behavior of different metals in smelting processes has existed and there are both technical and scientific challenges for the efficient use of secondary resources. It is possible to recover valuable metals to a great extent by collector copper metal/matte if the smelting conditions are favorable for their distribution to the matte/metal phase. The obtained data for the phase equilibria of copper/matte-slag-tridymite/spinel/wüstite-gas and the distributions of metals in the systems contribute to the determination of cost-effective ways for improving the recoveries of valuable trace metals from secondary materials through copper smelting processes and provided insight into improving smelting capability by adjusting the temperature, gas atmosphere, and flux. The present results are also useful for developing databases for simulating copper smelting processes and calculating the distributions of minor elements in copper smelting systems.

1.4 Thesis outline

The thesis consists of this compendium and six peer-reviewed scientific journal articles, attached as appendices at the end of the thesis. The compendium gives a brief introduction to the topic in the first chapter and to its research background in the second chapter, including a short description of the current industrial practices of pyrometallurgical WEEE recycling through copper smelting as well as a literature review on the phase equilibria of copper/matte and slag and prior studies on trace metal distributions. The third chapter presents the experimental procedures and analytical techniques used in this work. The final chapter provides a summary of the most important results regarding phase equilibria and trace metal distributions in various copper smelting system.

2. Background

2.1 Copper flash smelting

Copper mainly exists in the Earth's crust as sulfide minerals, such as chalcopyrite ($CuFeS_2$) and chalcocite (Cu_2S) [69]. The Cu-Fe-S sulfide minerals are difficult to treat via hydrometallurgical processes. Therefore, the extraction of copper from copper sulfide minerals is mainly accomplished through pyrometallurgical smelting technologies, including bath and flash smelting technologies.

The flash smelting technology developed by Outokumpu in 1949 in Harjavalta, Finland, for smelting copper sulfide concentrates was one of the most important innovations in pyrometallurgy [70]. Currently, around half of all copper matte smelting around the world is produced through Metso Outotec flash smelting, as it is known today. The advantages of flash smelting technology include: (1) the utilization of the exothermic reactions of the sulfide minerals with oxygen; (2) high concentrate throughput rates; (3) recovery and efficient use of off-gas heat with a heat recovery boiler; (4) dry dust recycling [69]. Because of these distinct advantages, flash smelting technology has also been adopted to a significant extent for nickel sulfide concentrate smelting. In copper flash smelting, the dried copper sulfide concentrates combined with fluxes and recycled materials are introduced into the flash smelting furnace (FSF), as shown in Figure 1. The copper sulfide concentrates are blown together with air/oxygen-enriched air into the reaction shaft, resulting in the rapid oxidation of Fe and S in the sulfide mineral at a typical smelting temperature of 1200-1350 °C, subsequently producing Cu-Fe-S matte with a typical copper concentration of 45-75 wt%. Silica is used to produce a fayalite slag and simultaneously decrease the activity of FeO in slag [72]. Two immiscible layers of molten matte and slag are formed in the settler of the FSF. The sulfur dioxide-rich off-gases are removed from the furnace through the uptake shaft and directed to the heat recovery boiler. The formation of matte and slag can be described using the following overall reactions:

$$CuFeS_2(s) + O_2 \rightarrow (Cu\text{-}Fe\text{-}S)_{matte} + (FeO)_{slag} + SO_2 \quad (1)$$

$$FeO(s) + SiO_2(s) \rightarrow (FeO{\cdot}SiO_2)_{slag} \quad (2)$$

In the current situation of copper ores of decreasing grade, more complex minerals and recycled materials are being introduced into flash smelting, leading to an increased slag volume containing more metals with high economic value and other new elements coming from recycled materials.

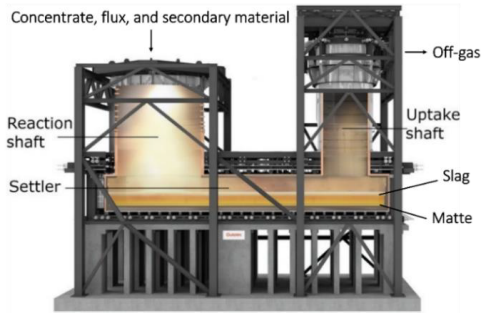

Figure 1. Schematic of the Metso Outotec flash smelting furnace [71].

2.2 Secondary copper smelting

The composition of WEEE varies from one product to another. Generally, the major materials in WEEE are metals and plastics, accounting for around 75-80% of the overall mass of the waste material, as shown in Figure 2. Table 1 shows a comparison of metal concentrations between different types of WEEE and primary ore. Copper, nickel, and precious metals occur in higher concentrations in WEEE than in primary ores. Among all the metals contained in WEEE, copper and precious/critical, rare metals are the main drivers for recycling, due to their high economic value. The copper-rich scrap contained in WEEE or from other secondary materials can be fed into a secondary copper smelter to remove impurities such as Fe and Sb by oxidation and recover many precious metals into the matte/copper alloy.

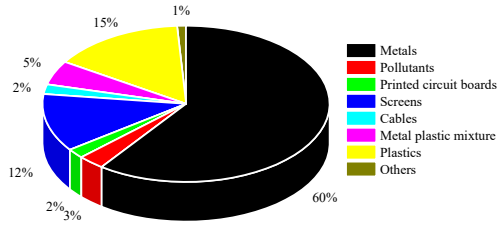

Figure 2. Material fractions in WEEE (Reproduced using data from the literature [73]).

Table 1. Concentrations of metals in typical WEEE and primary ore [1, 65].

Type	Concentration/wt%					Concentration/ppmw		
	Fe	Cu	Al	Pb	Ni	Ag	Au	Pd
Printed circuit boards	5.3	26.8	1.9	–	0.47	3300	80	–
TV board scrap	28	10	10	1	0.3	280	20	10
Mobile phone scrap	5	13	1	0.3	0.1	1380	350	210
Portable audio scrap	23	21	1	0.14	0.03	150	10	4
DVD player scrap	62	5	2	0.3	0.05	115	15	4
Calculator scrap	4	3	5	0.1	0.5	260	50	5
PC mainboard scrap	4.5	14.3	2.8	2.2	1.1	639	566	124
Printed circuit boards scrap	12	10	7	1.2	0.85	280	110	–
TV scrap (CRTs removed)	–	3.4	1.2	0.2	0.038	20	<10	<10
Average content in primary ore/wt%	30	0.5	30	4	1	0.01	0.0001	0.0001

Compared with primary copper smelters, a wider variety of scrap can be incorporated into secondary copper smelters and subsequently produce refined copper as well as valuable side products of multiple precious and critical elements [74]. Furthermore, the transportation costs of WEEE to a secondary copper smelter can be much less than those for a primary copper smelter (generally located close to a mine) since secondary copper smelters can be located near the scrap generation and collection site, e.g., close to cities with a large population. Among these secondary copper smelting routes, the processing of WEEE in TSL (top submerged lance) furnaces [75], such as the Ausmelt® and ISASMELT® technologies, is commonly used [76]. Secondary materials like WEEE, containing precious and trace elements, are introduced into the TSL furnace and the elements distribute in smelting into matte/black metal, slag, and gas phases. The following converting and refining operations, especially when conducted in the same furnace, can be energy-saving and effective recovery routes for extracting metal values from the valuable metals enriched in copper. Figure 3 shows one route for WEEE recycling that employs secondary copper smelting processes.

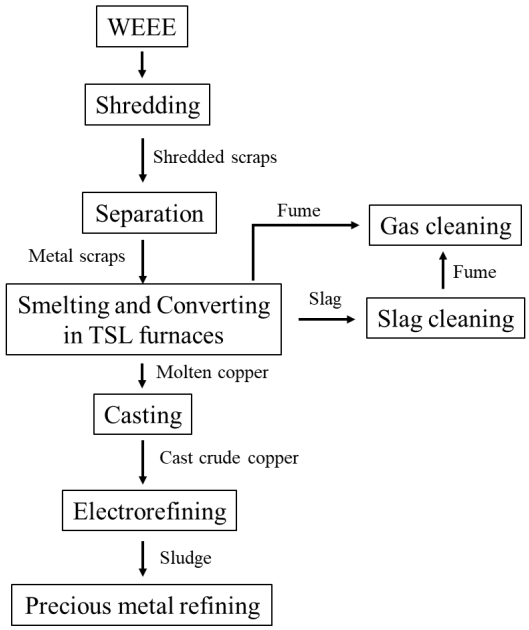

Figure 3. Schematic of WEEE recycling through secondary copper smelting.

2.3 WEEE recycling through copper smelting - industrial practice

2.3.1 Umicore's integrated metal smelter and refinery

Umicore's Hoboken plant recycles various kinds of metals from e-waste via a secondary copper smelting route. It is one of the world's largest precious metals recycling facilities with a production capacity of over 50 t platinum group metals (PGMs), over 100 t of gold, and 2400 t of silver [77]. The annual average capacity of feed materials at Umicore is more than 250,000 t [77], including industrial wastes, by-products from other non-ferrous smelters, printed circuit boards, and electronic components. Figure 4 shows the flowsheet for Umicore's integrated

metals smelter and refinery, consisting of pyrometallurgical, hydrometallurgical, and electrowinning processes. Generally speaking, the recycling operations at Umicore can be divided into two processes, i.e., Precious Metals Operation (PMO) and Base Metals Operation (BMO).

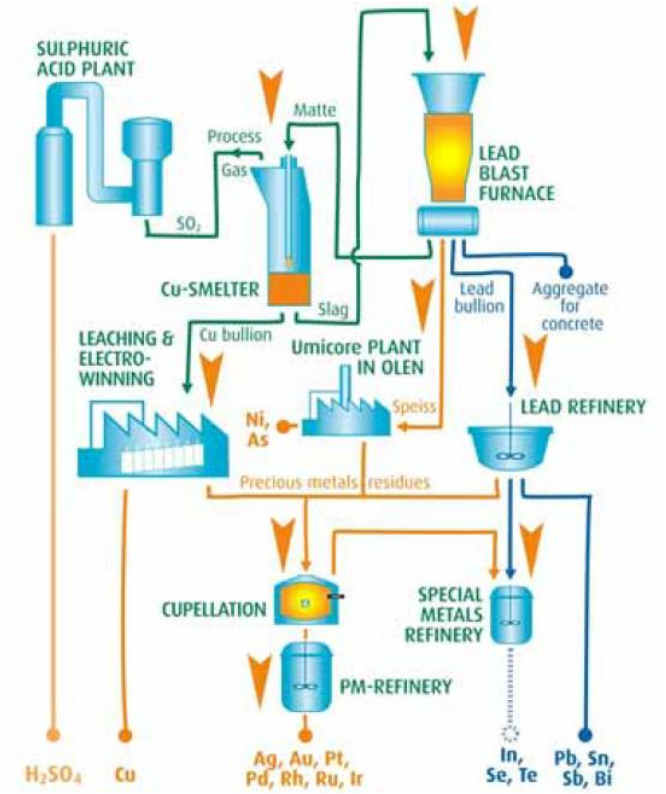

Figure 4. Schematic of the flowsheet for Umicore's integrated metals smelter and refinery [77].

The Precious Metals Operation (PMO) aims to recycle precious metals (PMs) from a wide range of complex secondary materials, including WEEE and other industrial wastes, that are processed in an ISASMELT furnace. Oxygen-enriched air and fuel are injected into the molten bath to oxidize the impurities, and coke is subsequently added to reduce the valuable metals. The combustion of plastic and other organic components supplies energy for smelting and partially replaces coke as the reducing agent. The energy supplied from WEEE plastics has been estimated to be >33000 MJ/t, and the concentrations of chlorinated dioxins/furans after off-gas cleaning are below the legal emission limit of 0.1 ngTEQ/Nm^3 [78], indicating a low impact on the environment. PMs are concentrated in the copper bullion and other impurities report to the lead slag. The PMs-rich copper bullion is subsequently treated by leaching and electrowinning. The PMs are collected in the leaching residue and then recovered by refining at the precious metals refinery.

The Base Metals Operation (BMO) aims to process the by-product from the PMO in a lead blast furnace, lead refinery, and special metals plant. The oxidized lead slag from the copper smelter and third-party materials with high lead concentration are fed into the lead blast furnace, producing lead bullion, nickel speiss, copper matte, and slag. The minor elements that follow the lead collector, such as In, Sn, and Te, are distributed into the impure lead bullion

and further treated in the lead refinery, producing pure lead, sodium antimonate, and residues containing special metals (selenium, tellurium, indium). The recovery of special metals from the residue is accomplished in the special metals refinery.

2.3.2 Boliden's Rönnskär plant

Boliden's Rönnskär plant treats copper and lead concentrates from its own mines and external mines as well as recycled copper scrap, e-waste, and other complex secondary raw materials. The annual recycling capacity for WEEE at the Rönnskär plant is more than 100,000 t [79]. Figure 5 shows the flowsheet of the plant with its copper and lead production lines. Copper mattes with matte grades of 65 wt% and 55 wt% Cu are produced in the FSF and electric smelting furnace (EF), respectively. The smelting of electronic scrap is carried out in the Kaldo furnaces (E-Kaldo plant and Kaldo plant). The copper matte from the FSF and the EF as well as the black copper from the Kaldo furnaces are further treated in a Peirce-Smith (PS) converter, which produces blister copper. The blister copper is subsequently refined in an anode furnace and cast as anode copper. Cathode copper (99.99% Cu) and anode slimes including precious metals are produced after electrorefining the anode copper in the electrolytic refinery. The recovery of PMs from anode slimes is carried out in the precious metals plant, where Ag granules, Au bars, palladium/platinum (Pd/Pt) concentrate, selenium (Se), and copper telluride (Cu_2Te) are produced after several processing steps.

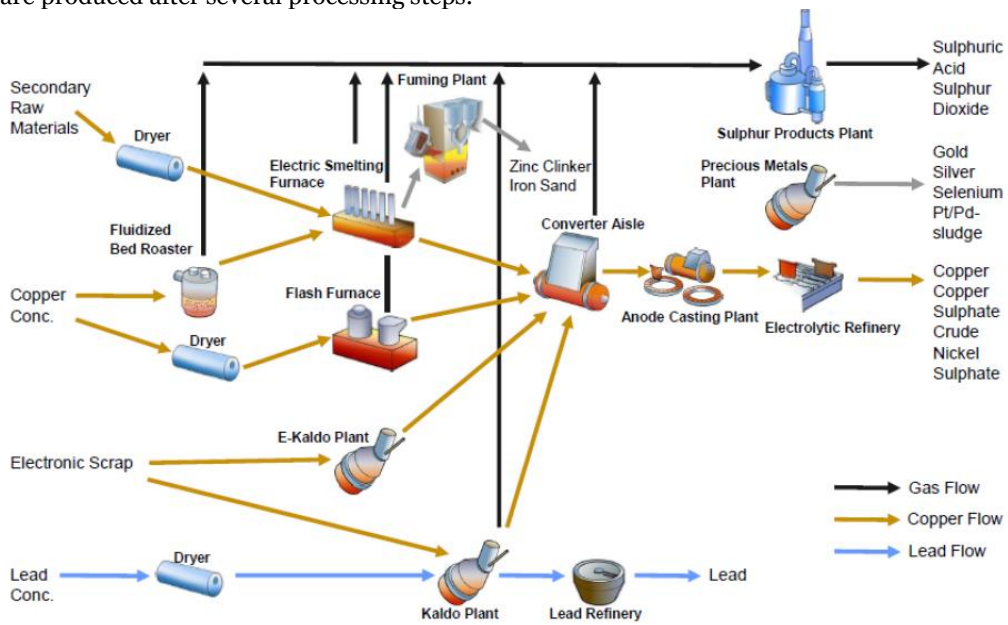

Figure 5. Flowsheet of Boliden's Rönnskär plant [79].

2.4 Phase equilibria in copper smelting

The Cu-Fe-O-SiO_2-(S-Al_2O_3-MgO-CaO) system plays an important role in pyrometallurgical copper smelting processes as it forms the basis for fayalite slags, copper alloys, and iron/copper-sulfide based mattes [43, 80, 81]. Accurate phase equilibrium information on the matte/metal-slag-tridymite/spinel/wüstite-gas systems as well as optimal control of slag

chemistry are of great interest for improving the industrial operation and performance of copper smelters.

Table 2 summarizes the details of the most recent experimental studies on matte/metal-slag equilibrium systems with/without minor elements under different experimental conditions. It can be seen that much effort has been devoted to the phase equilibria of metal/matte and FeO_x-SiO_2 slag at silica saturation and a low pSO_2 of 0.1-0.25 atm. Only a few experimental studies have been carried out at spinel (magnetite) saturation and to investigate the effects of basic oxides on the equilibrium systems. However, iron spinel is a common phase formed in copper smelting processes [68, 111-113], and the basic oxides of Al_2O_3, MgO, and CaO are introduced into fayalite-based copper smelting slags through their presence in the concentrate feed, flux, or secondary materials, such as WEEE [114]. Therefore, it is important to determine the phase compositions and relations of metal/matte-slag equilibrium systems under different process conditions (such as T, pO_2), saturation conditions, and the effects of slag modifiers (Al_2O_3, MgO, and CaO) on the system. Moreover, the pSO_2, generated by the slag and matte formation reactions, in the horizontal settler of the FSF is equal to the prevailing total pressure [115, 116]. Since the late 1970s, the smelting capacity of the FSF has been increased by 100-200% since technical oxygen (> 95% O_2) was adopted in copper smelting [3, 117], resulting in an increased SO_2 content of the off-gas to > 50 vol% SO_2. Therefore, accurate phase equilibrium information of the copper matte and slag under a pSO_2 higher than 0.1 atm is essential for stable and optimized operation.

During copper flash smelting, the behaviors of impurity/valuable metals have a strong relation to their thermodynamic properties. A good understanding of the thermodynamics of trace metals in copper smelting will provide insight for improving the recoveries of valuable metals in the feed materials. The process and experimental conditions, including temperature, gas atmosphere (pO_2, pSO_2), slag composition, saturation phase, etc. have an influence on the minor element behavior that must be understood in order to efficiently recover valuable elements and remove impurities. Generally, the high-temperature equilibrium reaction of a trace element Me between molten metal/matte and slag in copper smelting can be described using the following oxidation equation:

$$[\mathrm{Me}] + \nu/2\mathrm{O}_2 = (\mathrm{MeO}_\nu), \qquad (3)$$

where the valence of a trace element Me in slag equals 2ν, and the trace element in matte/metal and slag were designated as [Me] and (MeO_ν), respectively. The equilibrium reaction constant K for Reaction (4) can be defined as:

$$K = \frac{\mathrm{a}(\mathrm{MeO}_\nu)}{\mathrm{a}[\mathrm{Me}]\mathrm{P}_{\mathrm{O}_2}^{\nu/2}}, \qquad (4)$$

where a[Me] and a(MeO_ν) refer to the activities of Me and MeO_ν in metallic solution/matte and slag. The distribution coefficient of Me between phase A and phase B can be defined as:

$$\mathrm{L}_{\mathrm{Me}}^{\mathrm{A/B}} = \frac{[\text{wt pct Me}]_{\text{in A}}}{(\text{wt pct Me})_{\text{in B}}}, \qquad (5)$$

where [wt pct Me] and (wt pct Me) denote the concentrations of the trace element in phase A and B, respectively. As suggested by Takeda et al. [118], the distribution coefficient can be expressed further as:

$$\mathrm{L}_{\mathrm{Me}}^{\mathrm{A/B}} = \frac{[\mathrm{n_T}]_{\text{in A}}(\gamma_{\mathrm{MeO}_\nu})\mathrm{P}_{\mathrm{O}_2}^{-\nu/2}}{\mathrm{K}[\gamma_{\mathrm{Me}}](\mathrm{n_T})_{\text{in B}}}, \qquad (6)$$

where K represents the equilibrium constant of Equation (4) and n_T represents the total mole number of mono-cationic constituents in different phases. [γMe] and (γMeO_ν) refer to the activity coefficients of Me in phase A and B, respectively. By reorganizing Equation (6), the logarithmic distribution coefficient can be represented as:

$$\mathrm{Log_{10}L_{Me}^{A/B}} = \mathrm{Log_{10}}\frac{(\gamma_{MeO_\nu})[n_T]_{in\ A}}{K(n_T)_{in\ B}[\gamma_{Me}]} - \frac{\nu}{2}\mathrm{Log_{10}P_{O_2}}, \quad (7)$$

The concentration of Me in different phases is quite low, thus obeying Henry's law, $\mathrm{Log_{10}}\frac{(\gamma_{MeO_\nu})[n_T]_{in\ A}}{K(n_T)_{in\ B}[\gamma_{Me}]}$ can be regarded as a constant C at a fixed temperature and when n_T of both phases stay constant. Subsequently, Equation (7) can be further expressed as:

$$\mathrm{Log_{10}L_{Me}^{A/B}} = C - \frac{\nu}{2}\mathrm{Log_{10}P_{O_2}}, \quad (8)$$

where $-\frac{\nu}{2}$ is the slope of the linearly fitted relationship between $\mathrm{Log_{10}L_{Me}^{A/B}}$ and $\mathrm{Log_{10}P_{O_2}}$. For the trace metal distributions between metal and slag, the slope $-\frac{\nu}{2}$ can be used to determine the oxidation state of trace element Me in slag.

Much work has been done on investigating the distributions of selected minor elements (Au, Ag, Pt, Pd, Ni, Co, and Sn) in pyrometallurgical copper smelting processes [25-36, 42-52, 54-68]. However, most of the previous studies were carried out either at a low $p\mathrm{SO_2}$ or at Al-Fe spinel/silica saturation in slags. Only limited studies on trace metal distributions between metal/matte and spinel/wüstite-saturated slags can be found. Little effort has been devoted to the effects of $p\mathrm{SO_2}$, temperature, saturation, and flux additions on the distributions of minor elements. Further, the large samples used in previous studies led to difficulties in reaching equilibrium, and the use of chemical analysis in previous studies after the physical separation of different phases contributed to the existence of discrepancies among the data obtained. Therefore, the present study was initiated with the purpose of closing the gap between the previous studies and enriching the experimental thermodynamic data on trace metal distributions in copper smelting systems. The use of the direct phase analysis techniques, EPMA and LA-ICP-MS, in the present study for measuring the concentrations of trace metals in the equilibrated assemblages ensured the accurate acquisition of the chemically dissolved elements in each phase.

Table 2. A summary table of most recent experimental studies on matte/metal-slag equilibria with/without the minor elements investigated in the same way as in the present study.

Investigators and Ref.	Type of slag	Minor elements	Conditions	T/°C	Analytics
Matte-slag equilibrium system					
Sukhomlinov et al. [35]	Silica-saturated FeO_x-SiO_2-(Al_2O_3, CaO)	Sn	pSO_2 = 0.1 atm	1300	EPMA
Tavera et al. [42]	Silica-saturated FeO_x-SiO_2	/	pSO_2 = 0.1-1 atm	1150-1300	CA*
Kho et al. [48]	Magnesia-saturated FeO_x-SiO_2	Co	Not reported	1250	ICP-AES
Louey et al. [49]	Magnesia-saturated FeO_x-SiO_2	Ag, Sn	Not reported	1250	ICP-AES
Yamaguchi [52]	Magnesia-saturated FeO_x-SiO_2	Pt, Pd	pSO_2 = 0.1 atm	1300	ICP
Avarmaa et al. [37, 53]	Silica-saturated FeO_x-SiO_2	Ag, Au, Pt, Pd	pSO_2 = 0.1 atm	1250-1350	EPMA and LA-ICP-MS
Abdeyazdan et al. [82]	Silica-saturated FeO_x-SiO_2-MgO	/	pSO_2 = 0.25 atm	1200-1300	EPMA
Fallah et al. [51, 83-86]	Silica-saturated FeO_x-SiO_2-(CaO)	/	pSO_2 = 0.1-0.6 atm	1200-1300	EPMA
Shimpo et al. [87]	Silica-saturated FeO_x-SiO_2-(Al_2O_3, CaO)	/	Not reported	1200	CA*
Sineva et al. [88]	Silica-saturated FeO_x-SiO_2-(Al_2O_3, CaO, MgO)	/	pSO_2 = 0.25 atm	1200-1300	EPMA
Hidayat et al. [89]	Silica-saturated FeO_x-SiO_2-(Al_2O_3)	/	pSO_2 = 0.25 atm	1200	EPMA
Takeda [90]	Magnesia-saturated FeO_x-SiO_2	/	pSO_2 = 0.1 atm	1300	CA*
Roghani et al. [91-93]	Magnesia-saturated FeO_x-SiO_2-(CaO)	Ag	pSO_2 = 0.1-1 atm	1200-1300	CA*
Hidayat et al. [94-96]	Spinel-saturated FeO_x-SiO_2	Ag	pSO_2 = 0.25 atm	1200-1250	EPMA
Chen and Sun et al. [97-99]	Spinel-saturated FeO_x-SiO_2	/	pSO_2 = 0.3-0.6 atm	1180-1250	EPMA
Sineva et al. [100, 101]	Spinel-saturated FeO_x-SiO_2-(Al_2O_3, MgO, CaO)	/	pSO_2 = 0.1-0.6	1200	EPMA
Copper-slag equilibrium system					
Anindya et al. [21, 74]	Spinel-saturated FeO_x-SiO_2-CaO	Sn	pO_2 = 10^{-7} atm	1300	ICP-AES
Klemettinen et al. [25]	Spinel-saturated FeO_x-SiO_2-(K_2O)	Sn	pO_2 = 10^{-10}-10^{-5}	1300	EPMA and LA-ICP-MS
Avarmaa et al. [28, 29]	Silica/spinel-saturated FeO_x-SiO_2-(Al_2O_3, CaO)	Au, Ag, Pt, Pd	pO_2 = 10^{-10}-10^{-5}	1300	EPMA and LA-ICP-MS
Avarmaa et al. [31]	Spinel-saturated FeO_x-SiO_2-(Al_2O_3, CaO)	Sn	pO_2 = 10^{-10}-10^{-5}	1300	EPMA and LA-ICP-MS
Dańczak et al. [32, 33]	Spinel-saturated FeO_x-SiO_2-Al_2O_3-(MgO)	Co, Ni, Sn	pO_2 = 10^{-11}-10^{-8}	1300	EPMA and LA-ICP-MS
Sukhomlinov et al. [34]	Silica-saturated FeO_x-SiO_2	Co, Ni	pO_2 = 10^{-8}-10^{-4}	1250-1350	EPMA and LA-ICP-MS
Henao et al. [39]	Spinel/tridymite saturated FeO_x-SiO_2-Al_2O_3-MgO-CaO	/	pO_2 = $10^{-8.5}$ atm	1150-1350	EPMA
Hellstén et al. [61]	FeO_x-SiO_2 slag in Fe crucible	Au, Ag	Not reported	1200-1300	EPMA and LA-ICP-MS
Ilyushechkin et al. [102]	Spinel/dicalcium ferrite-saturated FeO_x-CaO	/	CO_2-H_2 atmosphere	1150-1250	EPMA
Nikolic et al. [81, 103-105]	Spinel/pseudo-wollastonite/dicalcium ferrite-saturated FeO_x-SiO_2-CaO	/	pO_2 = $10^{-5.0}$-$10^{-6.5}$ atm	1200-1300	EPMA
Hidayat et al. [106-108]	Spinel/tridymite/cuprite/delafossite/FeO_x-SiO_2-(Al_2O_3, MgO, CaO, ZnO)	/	pO_2 = 10^{-5}-10^{-8} or in inert gas atmosphere	1100-1400	EPMA
Shishin et al. [109]	Spinel/tridymite/pseudo-wollastonite/wüstite/olivine/lime-saturated FeO_x-SiO_2-CaO	/	Ar-CO atmosphere or in sealed silica ampoules	1080-1250	EPMA
Klemettinen et al. [110]	Al-Fe spinel-saturated FeO-SiO_2-Al_2O_3-(CaO)	/	pO_2 = 10^{-10}-10^{-5}	1300	EPMA

CA*: Chemical analysis.

3. Experimental

The lab-scale experiments were conducted in the following order: sample preparation, high-temperature isothermal equilibration, drop quenching in an ice-water mixture, and direct phase composition analysis using EPMA and LA-ICP-MS. The materials, apparatus, experimental procedures, and analytical methods used for all experiments are described in detail in this chapter.

3.1 Raw materials

Three different kinds of equilibrium systems have been investigated in this thesis, i.e., matte-slag-tridymite-gas, matte-slag-spinel-gas, and copper-slag-spinel/wüstite-gas systems. High purity powders were used to synthesize the copper matte, copper alloy, and slags. Detailed information regarding the chemicals used for all experiments is given in Table 3. The copper matte was prepared using Cu_2S and FeS, including 1 wt% of each trace metal. The copper alloy was prepared using metallic copper powder including 1 wt% of each trace metal, Ag, Ni, Co, and Sn. Oxide powders of Fe_2O_3, SiO_2, Al_2O_3, and CaO were used to prepare the initial slag mixtures. The trace metals contained in each equilibrium system investigated and the experimental conditions are shown in Table 4.

For the matte-slag equilibrium experiments, the gas atmosphere was controlled using a gas mixture of CO (99.99 vol%), CO_2 (99.999 vol%), SO_2 (99.99 vol%), and Ar (99.999 vol%), all from AGA-Linde or Woikoski Oy, Finland. Argon was used for increasing the total gas flow rate in the matte-slag systems and flushing the furnace after the experiments. The pO_2 and pS_2 of the gas phase were calculated based on the equilibrium constants of reactions (9)-(10).

$$2CO(g) + O_2(g) = 2CO_2(g) \quad (9)$$

$$O2(g) + 1/2S_2(g) = SO_2(g) \quad (10)$$

For the copper-slag equilibrium experiments, the gas atmosphere was controlled using a mixture of CO and CO_2 so that the CO/CO_2 ratio corresponded to a certain pO_2 at 1200-1300 °C. The gas atmospheres calculated with HSC [119] or MTDATA using the SGTE database [120, 121] for different target pO_2 and pS_2 values are listed in Table 5. Figure 6 shows an example of the comparison between the initial pSO_2 and the calculated equilibrium pSO_2 at 1250 °C based on the gas flows used (Table 5) in the matte-slag-spinel-gas equilibrium experiments. The calculated equilibrium pSO_2 was slightly lower than the initial pSO_2 in the feed gas mixture and the difference decreased with increasing oxygen partial pressure.

Three kinds of crucibles, i.e., silica, spinel, and wüstite, were used for supporting the samples. The silica crucibles (Finnish SpecialGlass Oy, Espoo, Finland) with a purity of > 99.98 wt%

were used for the matte-slag equilibrium experiments at silica saturation. For the copper/matte-slag equilibrium experiments at spinel/wüstite saturation, synthesized spinel/wüstite crucibles were used as the substrates. The spinel and wüstite crucibles were made of iron foil (thickness 0.25 mm, 99.5 wt%) which was folded into a crucible shape; the bottom was punched into a bowl shape using a hemispherical stamping rod and subsequently oxidized at 1250 °C and a pO_2 of 10^{-7} and 10^{-10} atm for 4 h, respectively. The compositions of the crucibles were verified by XRD and SEM-EDS, as well as by EPMA after the equilibrium experiments. The wüstite and magnetite phases were distinguished by using the atomic ratio of iron to oxygen measured by EPMA. It was regarded as wüstite (FeO) if the atomic ratio of iron to oxygen was close to 1, and with a lower ratio as magnetite (Fe_3O_4). The use of spinel or wüstite crucibles was determined based on the phase boundaries of the Cu-Fe-O-SiO_2 system at a certain temperature and pO_2. The use of primary phase material crucibles ensured the silica/spinel/wüstite saturation of the slags without introducing contaminants into the equilibrium systems.

Table 3. Materials used for synthesizing the copper matte and slag.

Material	Supplier	Purity/wt%
Fe_2O_3	Alfa Aesar	99.998 wt%
SiO_2	Alfa Aesar	-40 mesh, -99.995 wt%
CaO	Sigma-Aldrich	99.90 wt%
Al_2O_3	Sigma-Aldrich	99.99 wt%
FeS	Alfa Aesar	-100 mesh, 99.9 wt%
Cu_2S	Alfa Aesar	-200 mesh, 99.5 wt%
Cu	Alfa Aesar	-625 mesh, 99.9 wt%
Au	Alfa Aesar	99.96 wt%
Ag	Alfa Aesar	99.95 wt%
Pt	Alfa Aesar	99.99 wt%
Pd	Alfa Aesar	99.9 wt%
Ni	Alfa Aesar	-120 mesh, 99.996 wt%
Co	Alfa Aesar	-1.6 micron, 99.8 wt%
Sn	Alfa Aesar	-325 mesh, 99.8 wt%

Table 4. Detailed information for each investigated equilibrium system.

Equilibrium system	Trace metals included	Slag	Crucible
Matte-slag-tridymite-gas	Au, Ag, Pt, and Pd	FeO_x-SiO_2 FeO_x-SiO_2-Al_2O_3 FeO_x-SiO_2-Al_2O_3-CaO	Silica
Copper-slag-spinel/wüstite-gas	Ag, Ni, Co, and Sn	FeO_x-SiO_2	Spinel/wüstite
Matte-slag-spinel-gas	Ag, Ni, Co, and Sn	FeO_x-SiO_2 FeO_x-SiO_2-Al_2O_3 FeO_x-SiO_2-CaO	Spinel

Table 5. Calculated gas flow rates under different conditions for varying target pO_2 and pS_2.

Equilibrium system	Temperature/°C	Gas flow rates/(mL·min^{-1})				$Log_{10}pO_2$/atm	$Log_{10}pS_2$/atm	pSO_2/atm
		CO_2	CO	SO_2	Ar			
Matte-slag-tridymite-gas	1300	15	12	40	300	-8.07	-2.28	0.1
		35	12	40	300	-8.00	-2.45	
		55	12	40	300	-7.92	-2.63	
		55	9	40	300	-7.79	-2.86	
		55	6	40	300	-7.58	-3.27	
	1300	25	25	200	160	-7.56	-1.95	0.5
		25	15.5	200	140	-7.42	-2.15	
		30	12	193	148	-7.36	-2.30	
		100	8.5	200	90	-7.09	-2.83	
Matte-slag-spinel-gas	1250	98.6	4.8	100	200	-7.50	-3.41	0.25
		96.8	5.9	100	200	-7.62	-3.17	
		94.1	7.5	100	200	-7.75	-2.91	
		91	9	100	200	-7.84	-2.73	
		91.5	10.5	100	200	-7.9	-2.62	
Copper-slag-spinel/wüstite-gas	1200	226.3	73.7			-10.0		
		272	28			-9.0		
		290.5	9.5			-8.0		
	1250	177.5	122.5			-10.0		
		246.3	53.7			-9.0		
		280.6	19.4			-8.0		
		293.6	6.4			-7.0		
		296.4	3.6			-6.5		
	1300	263.3	36.7			-8.0		
		287.3	12.7			-7.0		
		292.7	7.3			-6.5		

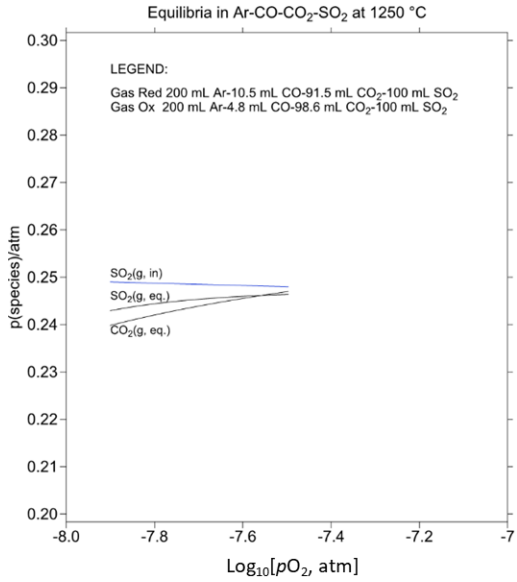

Figure 6. Comparison of the initial pSO_2 and the actual equilibrium pSO_2 at 1250 °C.

For the matte-slag-tridymite-gas equilibrium system, the experiments followed the molten slag-solid tridymite phase boundary in the FeO_x-SiO_2, FeO_x-SiO_2-Al_2O_3, and FeO_x-SiO_2-Al_2O_3-CaO systems in a controlled gas atmosphere. The phase diagrams of the FeO_x-SiO_2-Al_2O_3, and FeO_x-SiO_2-Al_2O_3-CaO systems at 1300 °C and a pO_2 of 10^{-10} to 10^{-5} and 10^{-8} to 10^{-6}, are shown in Figures 7 and 8, respectively. Based on the predictions of the phase boundaries calculated by MTDATA using the MTOX database [120, 121], the composition of each slag was selected as FeO_x/SiO_2 = 70/30, $FeO_x/SiO_2/Al_2O_3$ = 47/47/10, and $FeO_x/SiO_2/Al_2O_3$/CaO= 24/56/10/10.

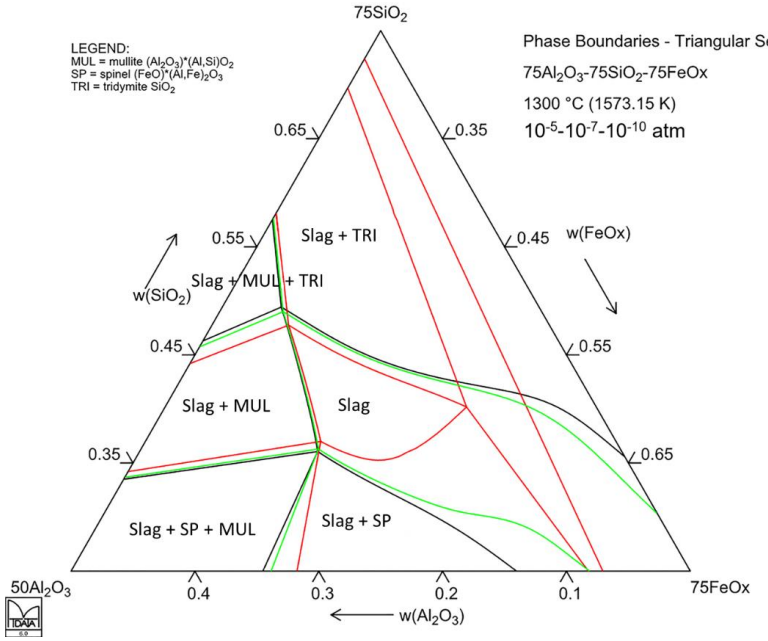

Figure 7. The isothermal sections of the FeO_x-SiO_2-Al_2O_3 system at pO_2 = 10^{-10} to 10^{-5} atm. SLAG-molten slag; FeO_x-FeO, $FeO_{1.333}$, or $FeO_{1.5}$; red line-pO_2 = 10^{-5} atm; green line-pO_2 = 10^{-7} atm; black line-pO_2 = 10^{-10} atm.

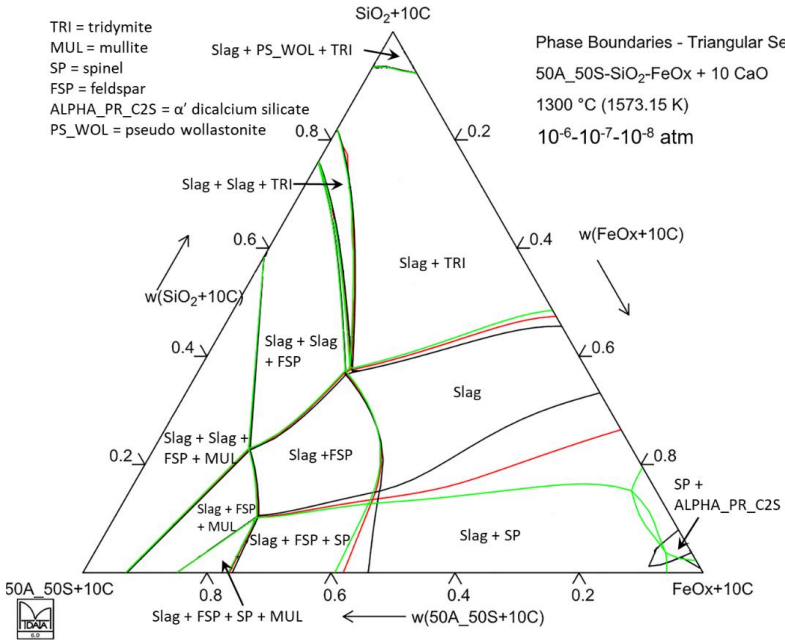

Figure 8. Isothermal section of FeO_x-SiO_2-$AlO_{1.5}$-10 wt% CaO system at pO_2 = 10^{-8} to 10^{-6} atm: OX_LIQ refers to molten slag; 10C refers to 10 wt% CaO; 50A_50S refers to (50 wt% $AlO_{1.5}$):(50 wt% SiO_2); FeO_x-FeO, $FeO_{1.333}$ or $FeO_{1.5}$; green line-pO_2 = 10^{-8} atm; red line-pO_2 = 10^{-7} atm; black line-pO_2 = 10^{-6} atm.

For the copper/matte-slag-spinel/wüstite-gas equilibrium system, the experiments followed the molten slag-solid spinel/wüstite phase boundary in the FeO_x-SiO_2, FeO_x-SiO_2-Al_2O_3, and FeO_x-SiO_2-CaO systems in equilibrium with a controlled gas atmosphere. The phase diagrams of the Cu-Fe-O-SiO_2 and FeO_x-SiO_2-CaO systems are shown in Figures 9 and 10, respectively, under varying conditions. Three FeO_x-SiO_2 slags with different initial compositions were used for the copper-slag-spinel/wüstite-gas equilibrium system, i.e., FeO_x/SiO_2 = 80/20, 85/15, and 90/10. The initial composition for each type of slag used for the matte-slag-spinel-gas equilibrium was Fe_2O_3/SiO_2 = 80/20, $Fe_2O_3/SiO_2/Al_2O_3$ = 62/28/10, and $Fe_2O_3/SiO_2/CaO$ = 62/28/10, respectively.

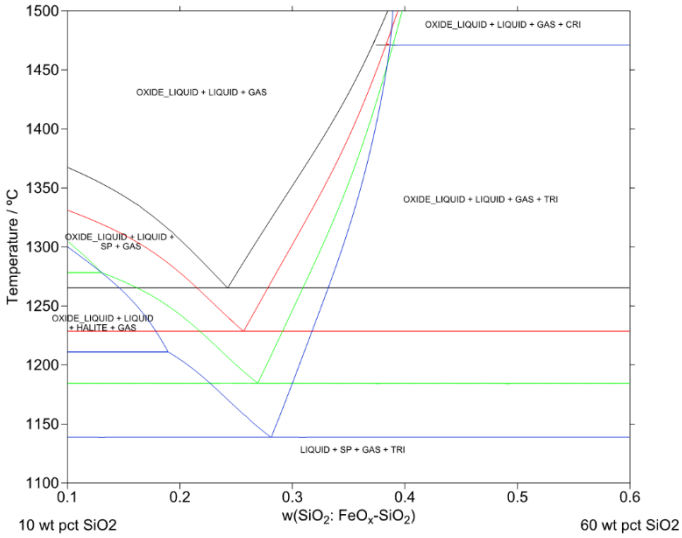

Figure 9. Cu-Fe-O-SiO_2 system calculated by MTDATA: blue line pO_2 = 10^{-9} atm; green line pO_2 = 10^{-8} atm; red line pO_2 = 10^{-7} atm; black line pO_2 = 10^{-6} atm.

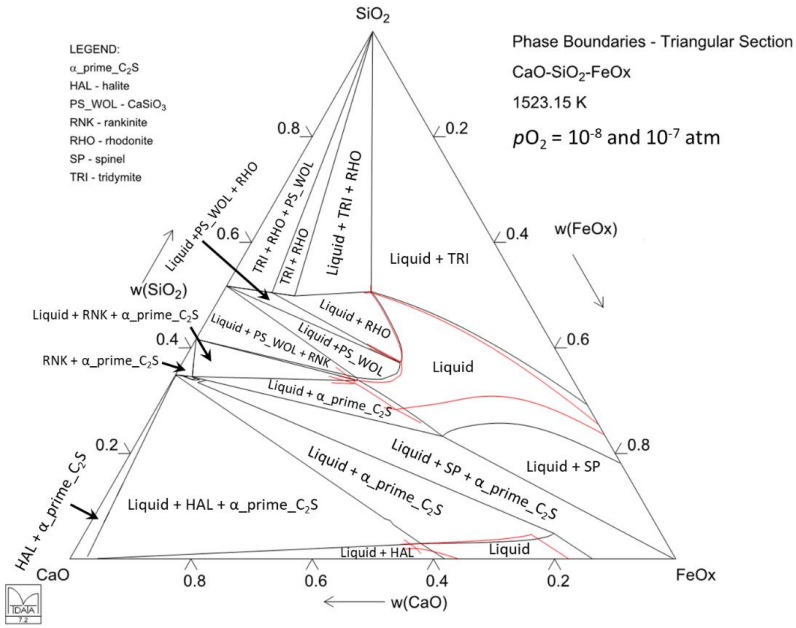

Figure 10. Phase diagram of the FeO_x-SiO_2-CaO system at 1250 °C and pO_2 of 10^{-8} to 10^{-7} atm: black line pO_2 = 10^{-8} atm; red line pO_2 = 10^{-7} atm.

3.2 Apparatus and methodology

The high-temperature isothermal equilibration experiments were conducted in vertical impervious alumina tube furnaces. A Lenton (PTF, 15/45/450) furnace equipped with SiC heating

elements was used for the matte-slag equilibrium experiments. Eurotherm 3216 PID controllers with three-zone temperature control were employed to regulate the temperature of the hot zone. The copper-slag equilibrium experiments were conducted in a Nabertherm furnace (Lilienthal, Germany, RHTV 120-150/1) fitted with $MoSi_2$ heating elements and a Naberthern P310 temperature controller. The temperature of the sample was measured using a calibrated S-type Pt/Pt-10 wt% Rh thermocouple (Johnson-Matthey Noble Metals, UK) located next to the sample and connected to a 2010 DMM multimeter (Keithley, USA). The cold junction was measured using a PT100 resistance thermometer (SKS Group, Finland) connected to a 2000 DMM multimeter (Keithley, USA). The temperature data were collected using an NI LabVIEW data logging program. DFC26 digital mass flow controllers (Aalborg, USA) were used to regulate the flow rates of all gases. Figure 11 shows a schematic diagram of the equilibrium furnace and the sample holding technique in the hot zone.

For each experiment, approximately 0.1-0.2 g of matte/copper mixture with an equal amount of slag was pressed into a sample pellet using a hydraulic press. The sample pellets were then placed in crucibles held by a platinum basket and lifted up into the cold zone of the furnace. The CO-CO_2-SO_2-Ar/CO-CO_2 gas mixtures were introduced into the furnace for 30 minutes to stabilize the gas atmosphere before equilibration. Subsequently, the sample was lifted up into the hot zone for equilibration using a platinum wire from the top of the furnace. After the sample reached equilibrium, the lower end of the working tube was immersed in an ice-water mixture and the rubber plug was removed. The samples were quenched into the ice-water mixture by pulling up the platinum wire from the top of the working tube so that the phase assemblages generated at high temperatures were retained at room temperature. The quenched samples were dried and mounted in epoxy. Cross-sections of the samples were prepared by grinding with abrasive sandpaper and polishing using a polishing cloth with a diamond spray. The polished sample surfaces were carbon coated using a carbon sputtering device. Two identical series were conducted to ensure the reproducibility of experiments.

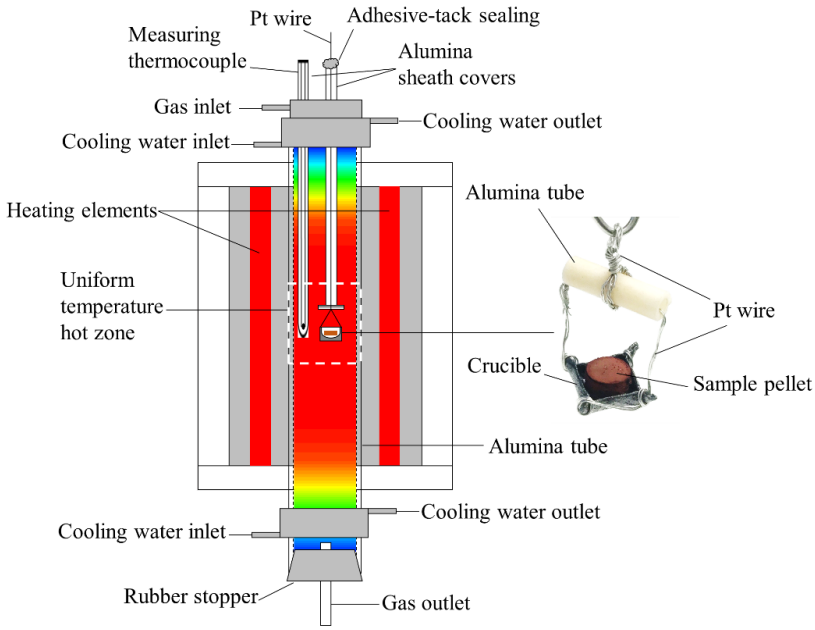

Figure 11. Equilibrium furnace used for the experiments (left) and the sample holding technique (right).

To determine the appropriate time for reaching homogeneous liquid and solid compositions, time series experiments were conducted for the different systems. The equilibration time was determined based on the stabilization of the matte/copper and slag compositions. For the matte-slag equilibrium system at silica/spinel saturation, the equilibration time was defined to be 4 h, whereas the copper-slag system reached equilibrium in 16 hours [29, 32, 33]. However, to ensure homogeneous concentrations of trace metals in all phases under all the conditions investigated, all samples were annealed for 24 h at the experimental temperature.

3.3 Analytical methods

3.3.1 SEM-EDS

The microstructure and phase compositions were pre-examined and photographed using a Tescan Mira 3 scanning electron microscope (SEM, Tescan, Brno, Czech Republic) equipped with an UltraDry silicon drift energy dispersive X-ray spectrometer (EDS, Thermo Fisher Scientific, Waltham, MA, USA) and NSS microanalysis software. The SEM-EDS analyses were executed with the following settings: working distance of 20 mm, accelerating voltage of 15 kV, beam current of 20 nA. Natural occurring minerals or synthetic metallic standards were used to calibrate the X-ray lines of different elements.

3.3.2 EPMA

The concentrations of major elements in all phases and the concentrations of trace metals in copper and matte were determined using a Cameca SX100 EPMA (Cameca SAS, Genevilliers, France) equipped with five wavelength dispersive spectrometers (WDS). For the matte-slag equilibrium systems at silica saturation, at least eight analysis points were selected from the well-quenched areas of each phase. Beam diameters of 100 μm and 50-100 μm were employed for the matte and slag phases, respectively. For the matte/copper-slag equilibrium at spinel/wüstite saturation, a three-spot analysis technique was used. A defocused beam diameter of 20 μm was used for the spinel/wüstite phase and a diameter of 50 μm for the copper and matte phase. Figure 12 gives an example showing the principle of selecting the individual analyzing spots from matte and slag phases. The results for point 1 from the slag phase are the average concentration measured from three spots: a, b, and c. Similarly, the reported value for point 1 in the matte phase was obtained by calculating the average concentration of spots A, B, and C. The standard deviation was calculated among all eight points from each phase. The use of the three-spot analysis technique decreased the standard deviations of the data and ensured the accurate determination of the chemically dissolved elements in all phases. The standard materials used in EPMA analyses were natural minerals or synthetic metals, as listed in Publications 1-6. The analytical parameters for EPMA analyses were an accelerating voltage of 20 kV and beam current of 60 nA. The typical totals of EPMA analyses were between 98 and 100.7. The detection limits of EPMA for trace metals in all phases were between 100 and 700 ppmw. However, the concentrations of some trace metals in matte/slag/spinel/wüstite were lower than the detection limits of EPMA, so they were subsequently measured by LA-ICP-MS. The PAP-ZAF online matrix correction program was used for the raw data processing [122].

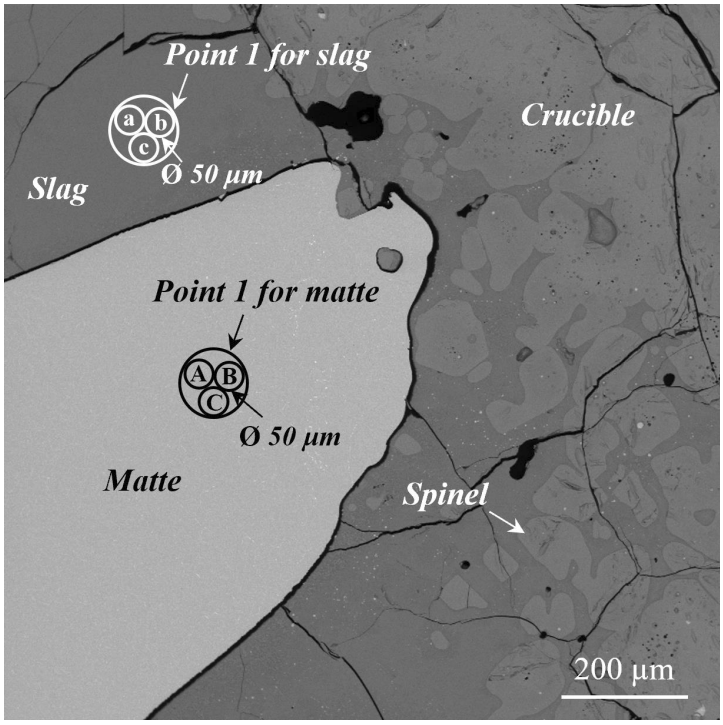

Figure 12. A schematic of the three-spot analysis technique used in EPMA analyses on the matte and slag phases.

3.3.3 LA-ICP-MS

The concentrations of trace metals in all slags and solid spinel/wüstite were measured by LA-ICP-MS housed at the Geological Survey of Finland (GTK). In the matte-slag-spinel-gas equilibrium system, the concentrations of cobalt and tin in matte were also measured using LA-ICP-MS. The setup used for the LA-ICP-MS analyses consisted of a Photon Machines Analyte Excite 193 nm ArF laser ablation device (Teledyne CETAC Technologies, USA) and a Nu AttoM single-collector ICP-MS system (Nu Instruments Ltd, UK). The laser ablation analyses were carried out at a pulse frequency of 10 Hz and pulse energy of 5 mJ to form an energy flux of 2.17-2.5 J/cm^2 on the sample surface. The laser beam spot size was chosen to be 40-65 µm, depending on the system and the size of the analyzed phases. The LA-ICP-MS analyses started with a 20 s baseline measurement followed by switching on the laser for 40 s with 350-400 ablation pulses for signal acquisition. The time-resolved analysis (TRA) signals were collected using the fast-scanning mode at low resolution ($\Delta M/M$ =300). GSE glass and NIST 612 SRM were used as the primary external standards for spinel/wüstite and slag, respectively. NIST 610, GSD, BHVO-2G, and USGS BCR-2G glasses were used as reference materials to monitor the equipment condition and data accuracy. The isotope ^{57}Fe was used as the internal standard for magnetite/wüstite and ^{29}Si was used for slag by employing the EPMA measurement results for Fe and Si, respectively. GLITTER™ [123] software, which allows for baseline subtraction, signal integration over a selected time window, and quantification using known concentrations of the external and internal standards, was used for time-resolved analysis signal processing. The isotopes used and the detection limits of LA-ICP-MS for all trace metals investigated in different equilibrium systems are listed in Table 6.

Table 6. Detection limits of LA-ICP-MS for the minor elements contained in different equilibrium systems/ppmw.

System	Phase	Isotope						
		^{197}Au	^{107}Ag	^{109}Ag	^{194}Pt	^{195}Pt	^{196}Pt	^{104}Pd
Matte-slag-tridymite-gas at pSO_2 of 0.1 atm	Slag	0.0007	0.0042	0.004	0.0015	0.0013	0.0018	0.0238
Matte-slag-tridymite-gas at pSO_2 of 0.5 atm	Slag	0.0009	0.003	0.003	0.0017	0.0017	0.0024	0.026
		^{107}Ag	^{60}Ni	^{59}Co	^{120}Sn			
Matte-slag-spinel-gas at pSO_2 of 0.25 atm	Matte	0.0094	0.1746	0.0142	0.0326			
	Slag	0.0052	0.1669	0.0126	0.039			
	Spinel	0.0066	0.1876	0.0148	0.0434			
		^{109}Ag	^{60}Ni	^{59}Co	^{120}Sn			
Copper-slag-spinel-gas	Slag	0.004	0.08	0.01	0.02			
	Spinel/Wüstite	0.004	0.09	0.01	0.03			

4. Results and Discussion

The main results for the phase equilibria of copper/matte and slag under different saturation conditions as well as the equilibrium distributions of both precious and high-tech metals in the copper smelting systems were acquired using the high-temperature isothermal equilibration/quenching/EPMA/LA-ICP-MS technique. High-temperature equilibrium experiments were conducted regarding different primary phase fields. In this chapter, the findings on the phase equilibria of copper/matte and slag corresponding to primary and secondary copper smelting processes are presented first, followed by a discussion of the distributions of precious and high-tech metals in the equilibrium systems.

4.1 Matte-slag-tridymite-gas equilibrium system

4.1.1 Phase equilibria of matte and silica-saturated iron silicate slags at pSO_2 of 0.1-0.5 atm

The phase equilibria of matte and silica-saturated iron silicate slags were investigated at 1300 °C and a pSO_2 of 0.1-0.5 atm. The typical microstructure of the matte-slag system in equilibrium with tridymite is shown in Figure 13. A large fraction of recrystallized silica crystals, i.e., tridymite (> 99 wt% SiO_2), was precipitated in the slags, attributed to the silica saturation caused by the silica crucible. All phases were homogeneous after rapid quenching, except for the matte, where copper-rich veins (90-97 wt% Cu) were found. The copper-rich veins were formed due to the insufficient quenching rate of the sulfur-deficient matte, as reported earlier [37, 55, 88].

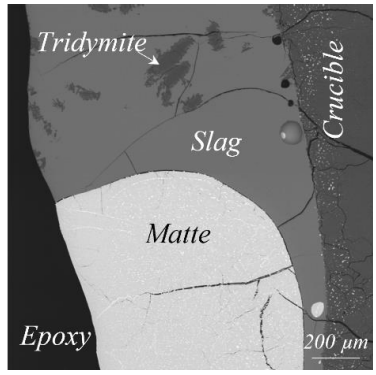

Figure 13. Back-scattered electron (BSE) image of the matte-slag-tridymite equilibrium system obtained at 1300 °C and pSO_2 of 0.1 atm.

The compositions of matte and slag obtained at 1300 °C and a pSO_2 of 0.1-0.5 atm are shown in Figure 14. The copper concentration in the matte increased with increasing oxygen partial pressure at a pSO_2 of 0.1 and 0.5 atm. Generally, the prevailing pO_2 increased with increasing pSO_2 at a given matte grade. Additions of Al_2O_3 and CaO into silica-saturated iron silicate slags led to an increase of copper concentration in the matte at a given pO_2. The Al_2O_3 and CaO additions decreased the activity of FeO in the slag at silica saturation, thus leading to an increase in the copper concentration in the matte. The concentrations of iron and sulfur in the matte displayed a similar decreasing trend with increasing matte grade, independent of slag modifiers. The sulfur concentration in the matte seems to be unaffected by the pSO_2, whereas a higher pSO_2 led to a small decrease of iron in the matte. The oxygen exhibited the lowest concentration in the matte, decreasing with an increasing copper content in the matte, which was probably independent of the partial pressure of SO_2 and the slag modifiers Al_2O_3 and CaO. The present results of iron concentration in the matte fitted well with the observations by Avarmaa et al. [37] but were approximately 4 wt% lower than the data in Fallah et al. [83]. The sulfur concentration in the matte obtained in this study agreed well with the results by Avarmaa et al. [37] but was around 2 wt% lower than the observations by Sukhomlinov et al. [35]. The different concentrations of trace metals in the matte contributed to the difference between the present study and the literature [35, 83].

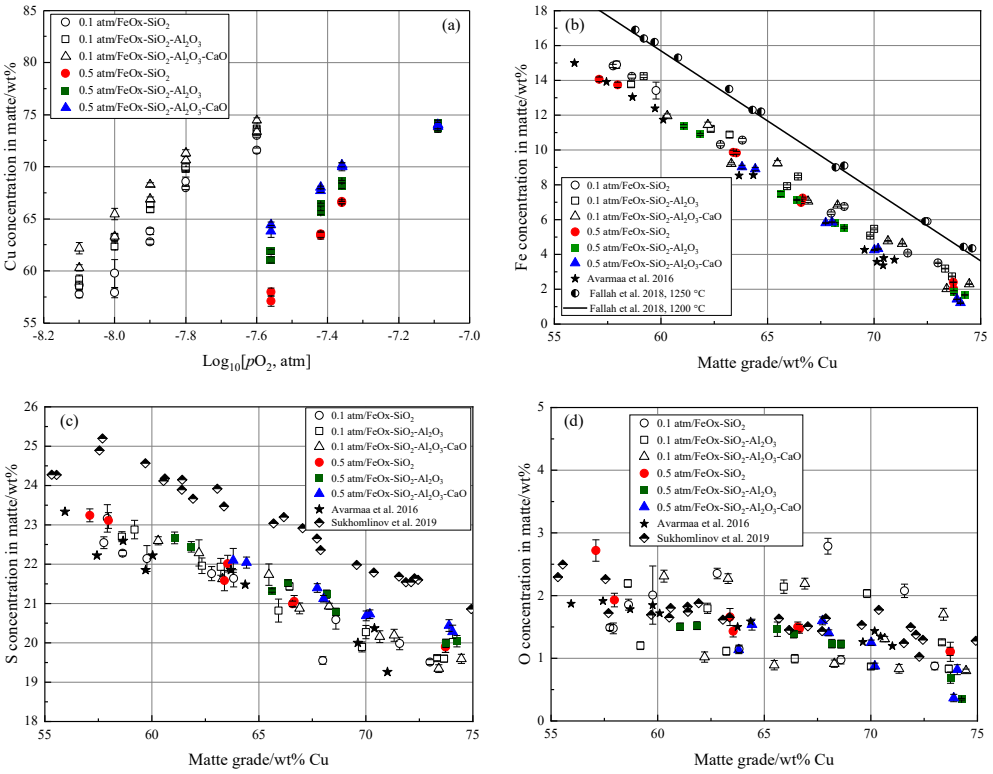

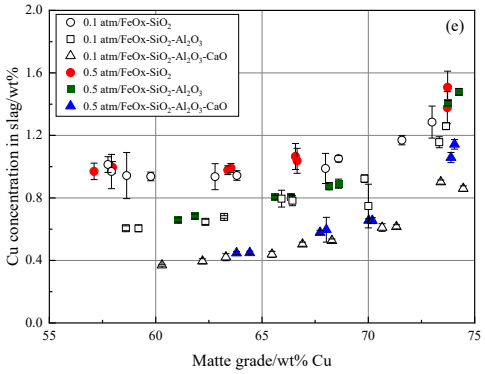
(e)
0.1 atm/FeOx-SiO2
0.1 atm/FeOx-SiO2-Al2O3
0.1 atm/FeOx-SiO2-Al2O3-CaO
0.5 atm/FeOx-SiO2
0.5 atm/FeOx-SiO2-Al2O3
0.5 atm/FeOx-SiO2-Al2O3-CaO
Cu concentration in slag/wt%
Matte grade/wt% Cu

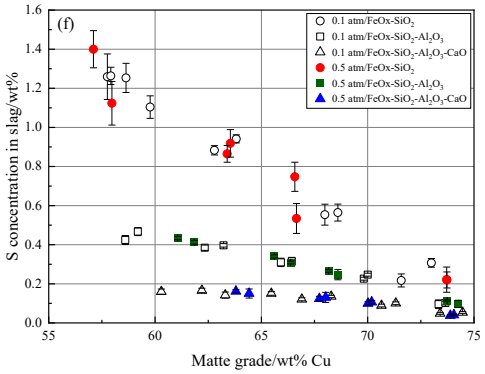
(f)
0.1 atm/FeOx-SiO2
0.1 atm/FeOx-SiO2-Al2O3
0.1 atm/FeOx-SiO2-Al2O3-CaO
0.5 atm/FeOx-SiO2
0.5 atm/FeOx-SiO2-Al2O3
0.5 atm/FeOx-SiO2-Al2O3-CaO
S concentration in slag/wt%
Matte grade/wt% Cu

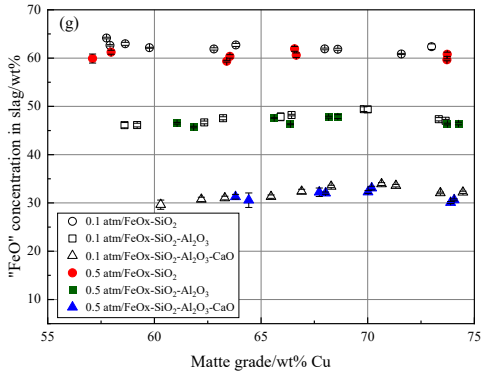
(g)
0.1 atm/FeOx-SiO2
0.1 atm/FeOx-SiO2-Al2O3
0.1 atm/FeOx-SiO2-Al2O3-CaO
0.5 atm/FeOx-SiO2
0.5 atm/FeOx-SiO2-Al2O3
0.5 atm/FeOx-SiO2-Al2O3-CaO
"FeO" concentration in slag/wt%
Matte grade/wt% Cu

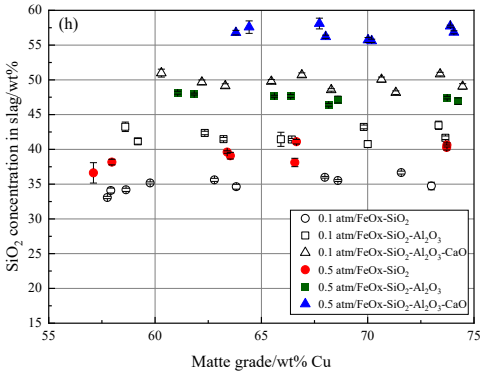
(h)
0.1 atm/FeOx-SiO2
0.1 atm/FeOx-SiO2-Al2O3
0.1 atm/FeOx-SiO2-Al2O3-CaO
0.5 atm/FeOx-SiO2
0.5 atm/FeOx-SiO2-Al2O3
0.5 atm/FeOx-SiO2-Al2O3-CaO
SiO2 concentration in slag/wt%
Matte grade/wt% Cu

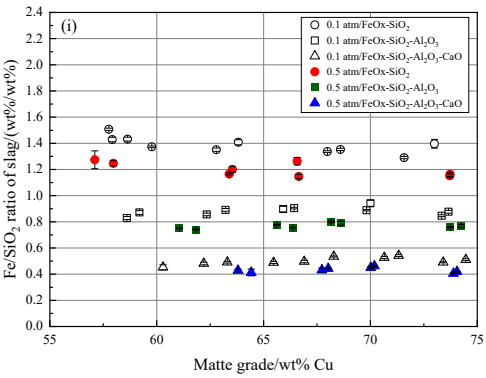
(i)
0.1 atm/FeOx-SiO2
0.1 atm/FeOx-SiO2-Al2O3
0.1 atm/FeOx-SiO2-Al2O3-CaO
0.5 atm/FeOx-SiO2
0.5 atm/FeOx-SiO2-Al2O3
0.5 atm/FeOx-SiO2-Al2O3-CaO
Fe/SiO2 ratio of slag/(wt%/wt%)
Matte grade/wt% Cu

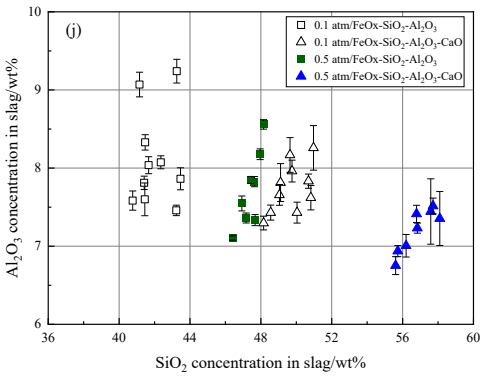
(j)
0.1 atm/FeOx-SiO2-Al2O3
0.1 atm/FeOx-SiO2-Al2O3-CaO
0.5 atm/FeOx-SiO2-Al2O3
0.5 atm/FeOx-SiO2-Al2O3-CaO
Al2O3 concentration in slag/wt%
SiO2 concentration in slag/wt%

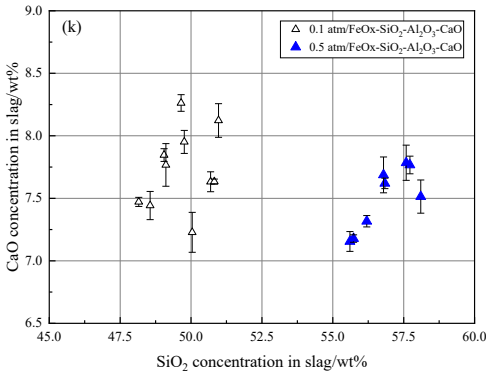

Figure 14. Matte and slag compositions at silica saturation as a function of matte grade or silica concentration in slag at 1300 °C and pSO_2 of 0.1-0.5 atm: (a)-(d) matte composition; (e)-(k) slag composition.

The copper concentration in all silica-saturated iron silicate slags increased with increasing matte grade, as reported in many other studies [35, 51, 67, 82-89]. The increase of the pSO_2 from 0.1 to 0.5 atm had no obvious impact on the copper loss in slags. However, the copper concentration in slags decreased with the addition of Al_2O_3 and CaO. The simultaneous addition of Al_2O_3 and CaO decreased the copper in the slag by 40-60% over the entire matte grade range investigated. The concentration of the chemically dissolved copper in the slag decreased due to the replacement of copper cations by Al^{3+} and Ca^{2+}. The sulfur concentration in all slags decreased with increasing matte grade, as reported in the literature [35, 51, 67, 82-89, 94-101]. Additions of Al_2O_3 and CaO into the silica-saturated slags decreased the sulfur concentration in the slag dramatically. It seems that the sulfur concentration in the slag was not affected by the prevailing pSO_2 of the equilibrium system. The "FeO" concentration in all silica-saturated iron silicate slags remained almost constant within the matte grade range studied, independent of the pSO_2. The silica concentration in the FeO_x-SiO_2 slag displayed a slightly increasing trend with increasing matte grade, but the results for the Al_2O_3- and CaO-containing slags had no significant changes over the matte grade. The increase of pSO_2 from 0.1 to 0.5 atm resulted in an increase in silica concentration in all silica-saturated slags at a fixed matte grade. The Fe/SiO_2 ratio in the FeO_x-SiO_2 slag showed a slightly downward trend with increasing matte grade, whereas the results for the Al_2O_3- and CaO-containing slag showed no obvious changes. The equilibrium concentrations of Al_2O_3 and CaO in the silica-saturated slags increased with the increasing silica concentration in the slags, suggesting that more silica is needed to attain a fully molten slag when increasing the concentrations of Al_2O_3 and CaO in the slags.

4.1.2 Precious metals distributions between matte and silica-saturated iron silicate slags at pSO_2 of 0.1-0.5 atm

The distributions of the precious metals Au, Ag, Pt, and Pd between the copper matte and silica-saturated iron silicate slag were investigated over a wide matte grade range of 55-75 wt% Cu from 0.1 to 0.5 atm pSO_2 at 1300 °C. The concentrations of all precious metals in the matte and slag were accurately measured by EPMA and LA-ICP-MS, respectively. The concentration of precious metals in matte and slag is shown in Figure 15 as a function of matte grade at 1300 °C and a pSO_2 of 0.1-0.5 atm.

The concentrations of all precious metals in the matte had no significant changes over the matte grade, and the slag modifiers had little effect on the precious metal concentrations in the matte. The increase of the pSO_2 from 0.1 to 0.5 atm had no significant impact on the concentration of Pd in the matte, whereas the concentration of Au, Ag, and Pt in the matte increased by approximately 0.1, 0.1, and 0.2 wt%, respectively, with increasing pSO_2.

Generally, the concentrations of all precious metals in the slags were extremely low, with the highest concentrations being for Ag, which varied between 25 and 100 ppmw. The concentrations of all precious metals in the slags were independent of the pSO_2. The concentrations of Au, Pt, and Pd in silica-saturated FeO_x-SiO_2 slag displayed similar downward trends with increasing matte grade. Additions of Al_2O_3 and CaO into silica-saturated iron silicate slags effectively decreased the dissolution of Au, Pt, and Pd in slags, down to as little as 0.5 ppmw. Ag had the highest concentration in the present silica-saturated iron silicate slags compared with the other precious metals investigated. The Ag concentration in the present FeO_x-SiO_2 slag remained nearly constant at around 60 ppmw over the entire matte grade range studied, whereas the results for Ag in the FeO_x-SiO_2-Al_2O_3 and FeO_x-SiO_2-Al_2O_3-CaO slags displayed increasing trends with increasing matte grade. The simultaneous addition of CaO and Al_2O_3 into the silica-saturated iron silicate slag decreased the Ag concentration in slag; however, the impact of a sole Al_2O_3 addition was not evident.

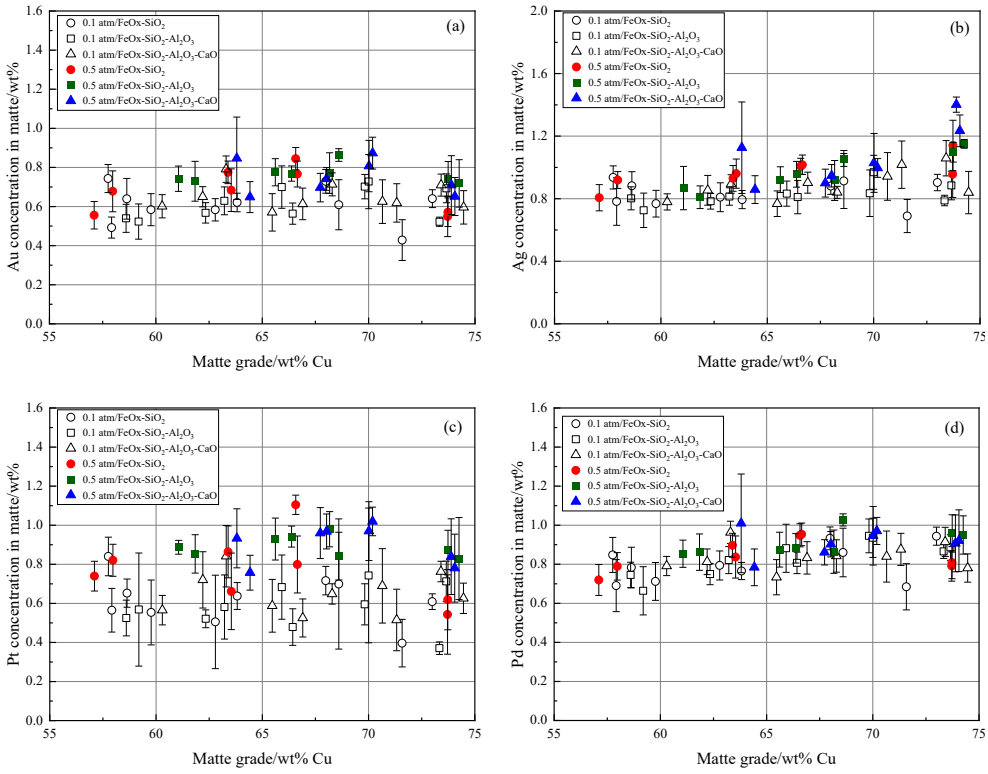

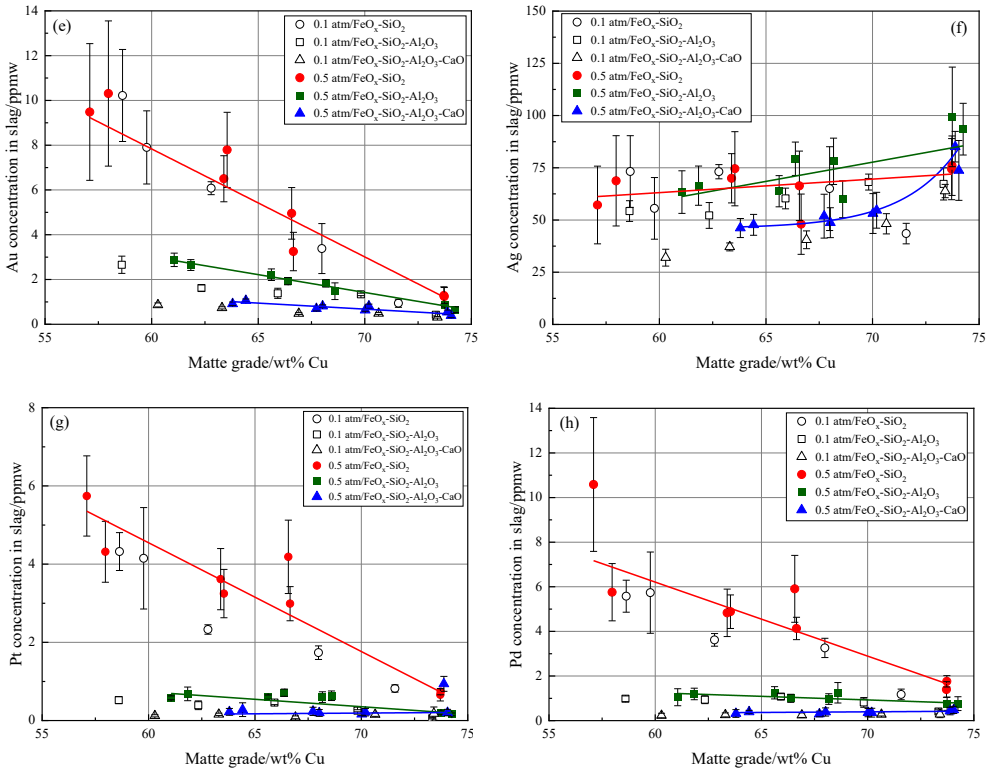

Figure 15. Concentrations of precious metals in matte and silica-saturated iron silicate slags vs. matte grade: (a)-(d) precious metals in matte; (e)-(h) precious metals in slag.

The logarithmic distribution coefficients of precious metals between matte and silica-saturated iron silicate slags calculated based on the experimental results are shown in Figure 16. The majority of all precious metals reported to the matte, with $L^{m/s} > 10^2$ in all cases, and the matte grade had different impacts on their distribution. The prevailing partial pressure of sulfur dioxide was found to have no significant impact on the distribution of precious metals between matte and silica-saturated iron silicate slags. The transfer of Au into the matte in equilibrium with all the types of slags investigated was favored by increasing matte grade, similarly to the results by Avarmaa et al. [53]. The logarithmic distribution coefficients of Pt and Pd between matte and FeO_x-SiO_2/FeO_x-SiO_2-Al_2O_3 slag displayed similar increasing trends with increasing matte grade. However, the distributions of Pt and Pd between matte and CaO-containing slag showed no significant changes as a function of matte grade. Additions of Al_2O_3 and CaO into silica-saturated iron silicate slags favored the transfer of Au, Pt, and Pd into the matte.

Ag exhibited different distribution behavior from the other precious metals investigated in this study. The logarithmic distribution coefficient of Ag between matte and FeO_x-SiO_2 slag stayed almost constant at 2.2 over the whole matte grade range studied. However, the distribution results for Ag between matte and Al_2O_3-/CaO-containing slags decreased with increasing matte grade. The addition of Al_2O_3 into silica-saturated iron silicate slag was observed to have no evident impact on the transfer of Ag into the matte, whereas CaO somehow improved the distribution of Ag into the matte. The present logarithmic distribution coefficient results for Ag were close to the data of Avarmaa et al. [53] but lower than the observations by Rogani et al. [92, 93]. The logarithmic distribution coefficients of Pt and Pd reported by Yamaguchi

[52] remained almost constant at approximately 3 over the matte grade range of 40-65 wt% Cu, after which they started to decrease with increasing matte grade.

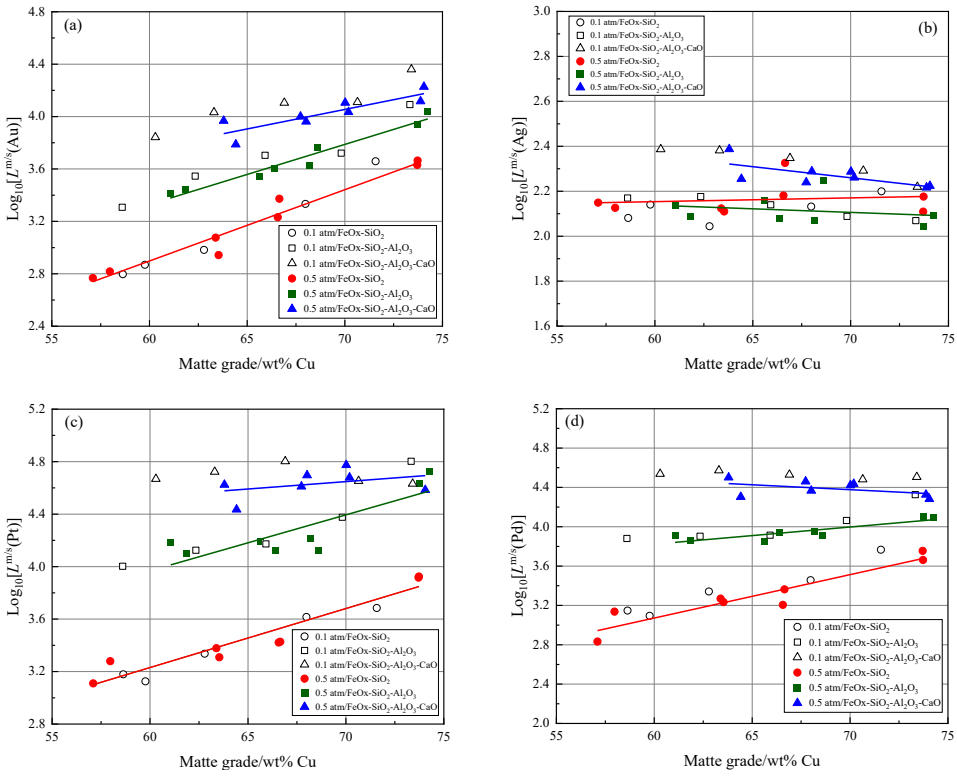

Figure 16. Logarithmic distribution coefficients of precious metals between matte and silica-saturated iron silicate slags vs. matte grade at 1300 °C and pSO_2 of 0.1-0.5 atm: (a)-Au; (b)-Ag; (c)-Pt; and (d)-Pd.

4.2 Copper-slag-spinel/wüstite-gas equilibrium system

4.2.1 Phase equilibria of copper and FeO_x-saturated iron silicate slag

The equilibrium phase relations between metallic copper alloys and spinel/wüstite-saturated iron silicate slags, which are related to the secondary copper smelting process, were studied at 1200-1300 °C. All experiments were conducted using synthesized spinel/wüstite crucibles. Figure 17 shows the typical microstructures of copper-slag-spinel/wüstite-gas equilibria at 1200-1300 °C. The copper alloy was homogeneous, whereas entrained copper droplets were observed in the slag, which were aggregated to the edges of the spinel/wüstite crystals, as shown in Figure 17(a). Figures 17(b) and (c) represent the well- and poor-quenched slag, respectively. The primary solid crystals, including the bulk continuous layer and discrete crystals, were stable at high temperatures. The discrete primary crystals had a euhedral shape with typical sizes ranging from 10 to 100 μm. In contrast, the secondary spinel/wüstite crystals, formed during quenching, displayed dendritic structures with a size of less than 10 μm, as shown in Fig. 17(c).

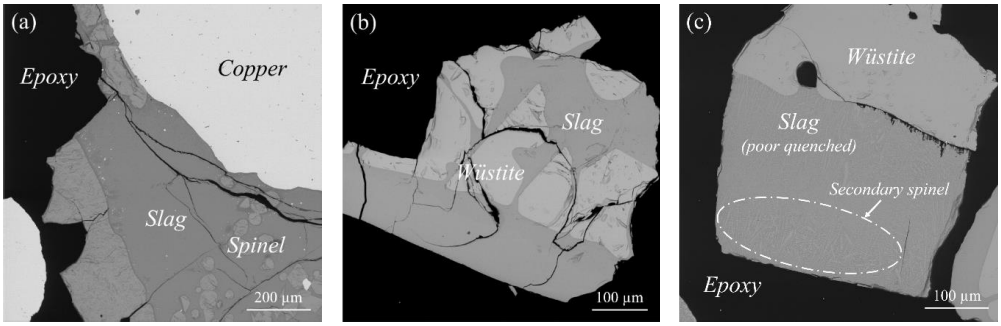

Figure 17. Typical BSE images of copper-slag-spinel/wüstite equilibrium at 1200-1300 °C.

The compositions of copper alloy and spinel/wüstite-saturated iron silicate slag at 1200-1300 °C as a function of oxygen partial pressure are shown in Figure 18. The copper concentration in the molten alloy phase increased with increasing pO_2 at all the temperatures investigated, mostly due to the oxidation of impurities into the slag. The temperature had no evident effect on the copper concentration in the metal alloy phase. The iron concentration in the metal decreased with increasing pO_2, due to its oxidation to the slag phase, and the influence of pO_2 on the iron concentration in the metal decreased at higher pO_2. The iron concentration in the metal increased with increasing temperature at a given pO_2.

The copper concentration in the slag at all temperatures investigated increased with increasing pO_2. At a given pO_2, the copper concentration in the slag decreased with increasing temperature. The effect of temperature on decreasing the copper concentration in the slag increased with increasing pO_2. Both the "FeO" and SiO_2 concentrations in the slag were greatly influenced by the pO_2 and temperature. The "FeO" concentration in the present spinel/wüstite-saturated iron silicate slag decreased with increasing pO_2. The increase in temperature resulted in an increase of the "FeO" concentration in the slag at the fixed pO_2. The SiO_2 concentration in the slag showed an upward trend with increasing pO_2 and decreased with increasing temperature at a given pO_2. The Fe/SiO_2 ratio in the present spinel/wüstite-saturated iron silicate slag increased with decreasing pO_2 at all the temperatures investigated.

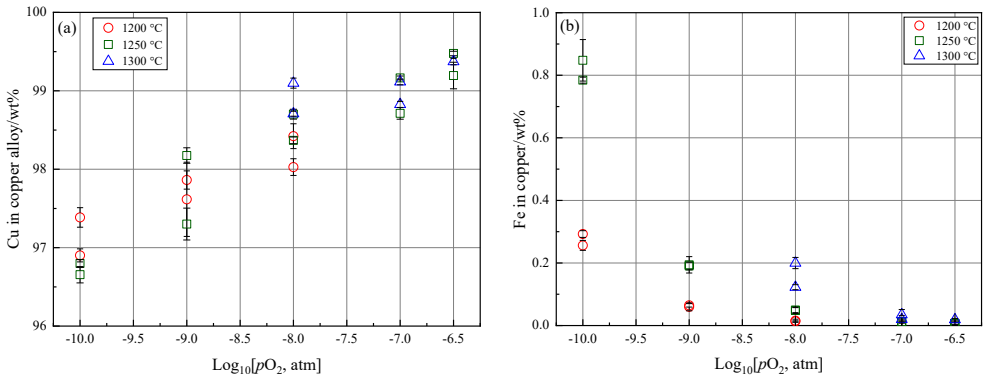

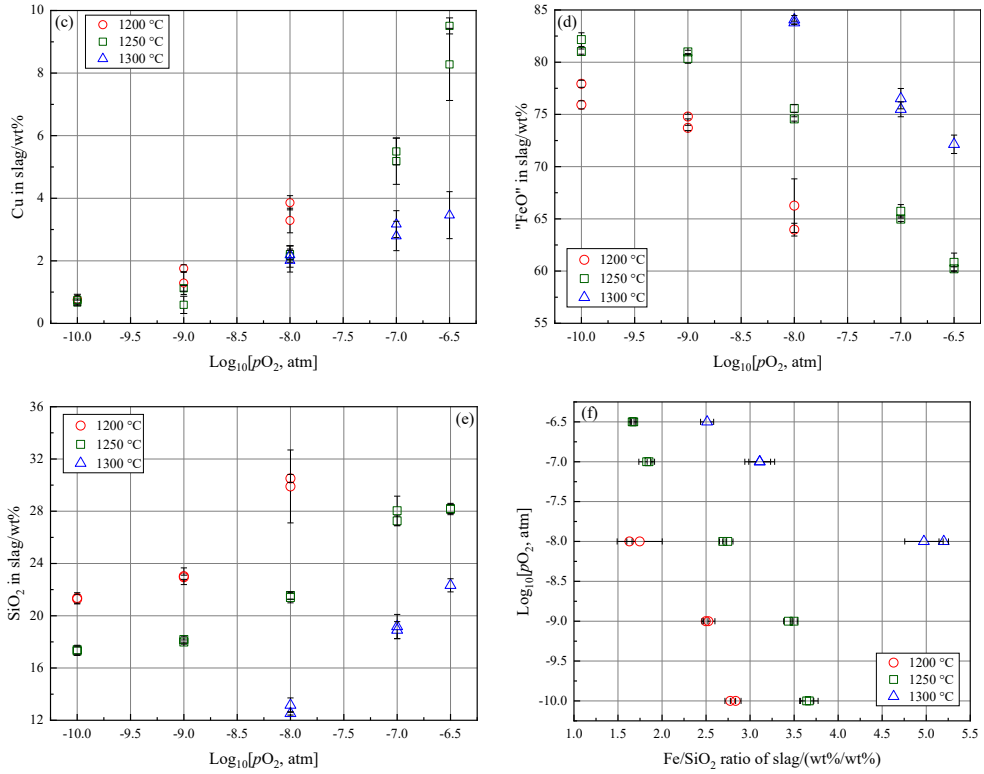

Figure 18. Equilibrium compositions of copper alloy and spinel/wüstite-saturated iron silicate slags at 1200-1300 °C: (a)-(b) copper alloy composition; (c)-(f) slag composition.

4.2.2 Precious/high-tech metal distributions between copper and spinel/wüstite-saturated iron silicate slag

The distribution behavior of Ag, Ni, Co, and Sn between the copper alloy and spinel/wüstite-saturated iron silicate slags was studied at 1200-1300 °C and a pO_2 of 10^{-10} to $10^{-6.5}$ atm, simulating the secondary copper smelting process. The dissolution of precious/high-tech metals in the solid spinel/wüstite primary phases was investigated by LA-ICP-MS for the first time in this study. The concentrations of precious/high-tech metals in copper, slag, and solid spinel/wüstite phases are shown in Figure 19.

The concentrations of Ag in the copper alloy were scattered compared with the high-tech metals investigated in this study. The increase of temperature from 1200 °C to 1300 °C led to a decrease of Ag in the copper alloy of approximately 0.8 wt%, indicating that the vaporization of Ag intensified at higher temperatures, as also reported in recent studies [28, 29, 34, 37, 53]. The Ni concentrations in the copper alloy displayed linearly decreasing trends with increasing pO_2. The increase in temperature from 1250 °C to 1300 °C resulted in an increase in Ni concentration in the copper alloy of around 0.1 wt%. The concentrations of Co in the copper alloy were significantly lower than those of the other metals investigated, with a decreasing trend against increasing pO_2. The increase in temperature favored the transfer of Co to the copper alloy. The results for Sn in the copper alloy displayed similar decreasing trends as Co, although

the effect of temperature on the transfer of Sn to the copper alloy was not as significant as for the other metals in this study.

Ag displayed the lowest concentration in all the spinel/wüstite-saturated slags in equilibrium with a copper alloy. The Ag concentration in the slag decreased with increasing temperature at a given pO_2. The effect of temperature on the concentration of Ag in the slag became stronger at higher pO_2 values. The Ni concentration in the slag displayed similar increasing trends as Ag. The present results for Ni in the slag decreased with increasing temperature at a fixed pO_2. The concentration of Co in the slag displayed a non-linear but increasing trend with increasing pO_2. The influence of higher temperature on decreasing the Co concentration in the slag was more significant in the lower pO_2 range of 10^{-10} to 10^{-8} atm. The concentration of Sn in the slag increased significantly with increasing pO_2 at 1200 °C. At 1250 °C, the concentration of Sn in the slag in the most oxidizing conditions was twice as high as that in the reducing conditions. However, the results obtained at 1300 °C showed no significant changes over the entire pO_2 range studied. The increase of temperature from 1200 °C to 1250 °C reduced the Sn concentration in the slag substantially at pO_2 values higher than 10^{-10} atm, owing to its stronger volatilization in more oxidizing conditions, whereas the temperature had much less effect on the Sn concentration between 1250 °C and 1300 °C.

The Ag concentration in the solid spinel/wüstite phase was extremely low (< 1 ppmw) when compared with the high-tech metals. The results for Ni, Co, and Sn displayed similar increasing trends with increasing pO_2, although the losses of Ni and Co in the spinel/wüstite phase were higher than that of Sn. The effect of higher temperature on decreasing the concentration of high-tech metals in spinel/wüstite was evident for all the minor elements, although less clear for Ag between 1250 °C and 1300 °C.

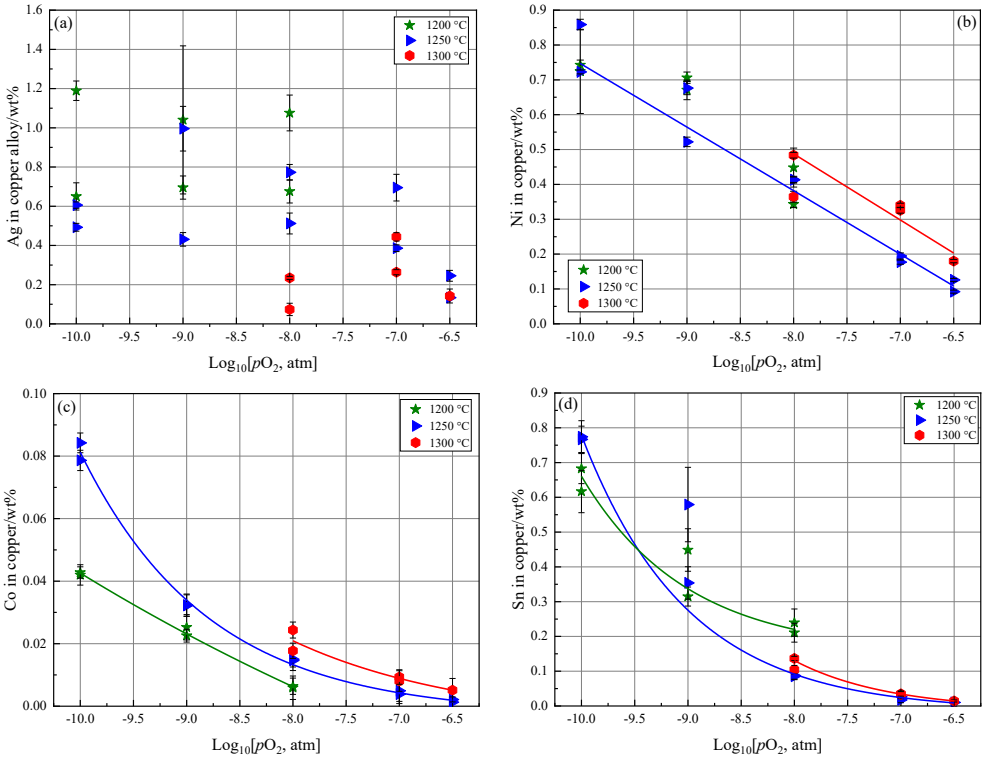

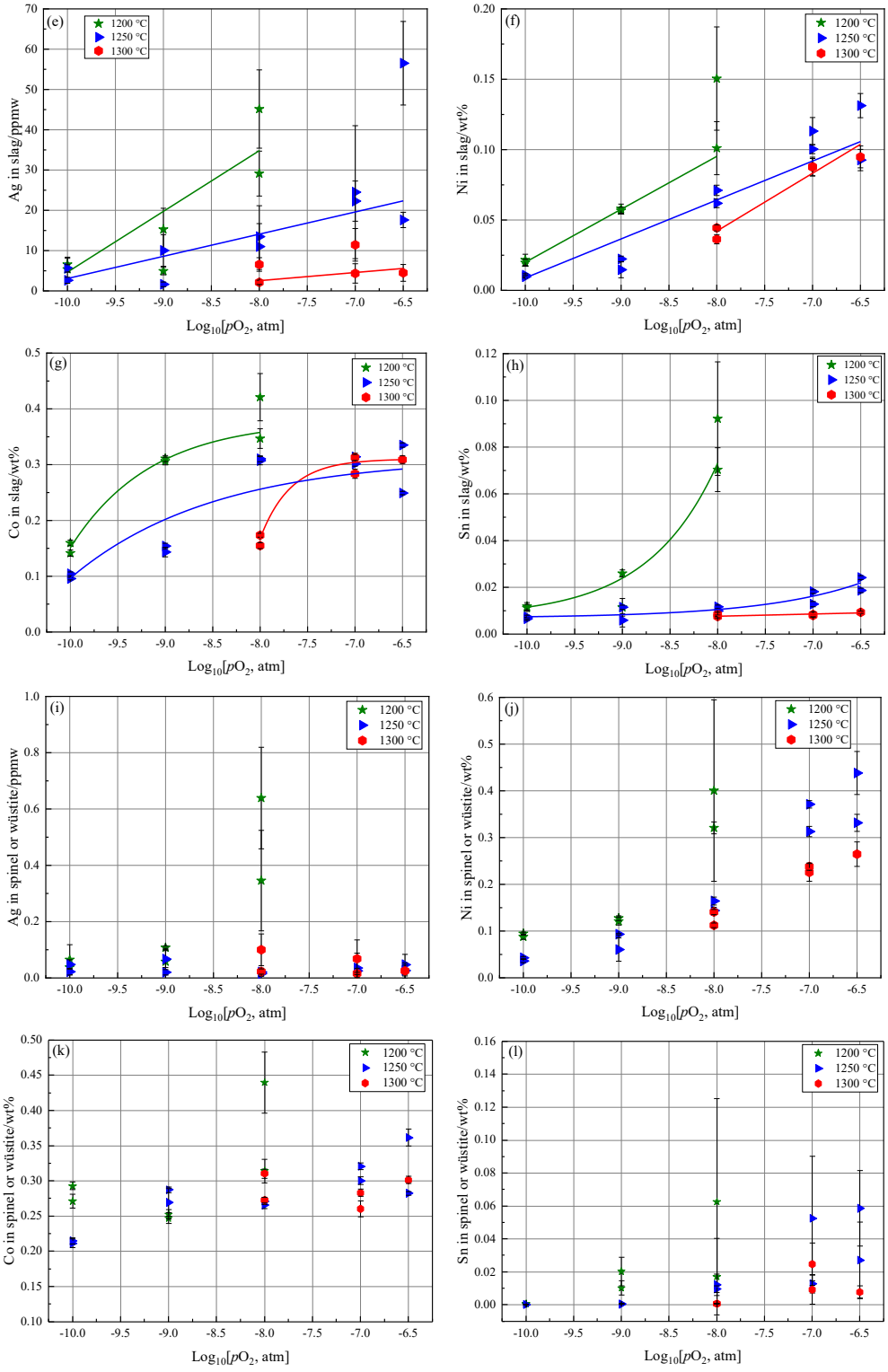

Figure 19. Concentrations of trace metals in metal, slag, and solid phases at 1200-1300 °C: (a)-(d) trace metals in metal; (e)-(h) trace metals in slag; (i)-(l) trace metals in solids.

The logarithmic distribution coefficients of precious/high-tech metals between copper alloy (Cu) and slag (S), $Log_{10}L^{Cu/S}[Me]$, as a function of logarithmic pO_2 are displayed in Figures 20(a)-(d). Figures 20(e)-(h) present the logarithmic distribution coefficients of precious/high-tech metals between solid spinel/wüstite and slag, $Log_{10}L^{Solid/S}[Me]$.

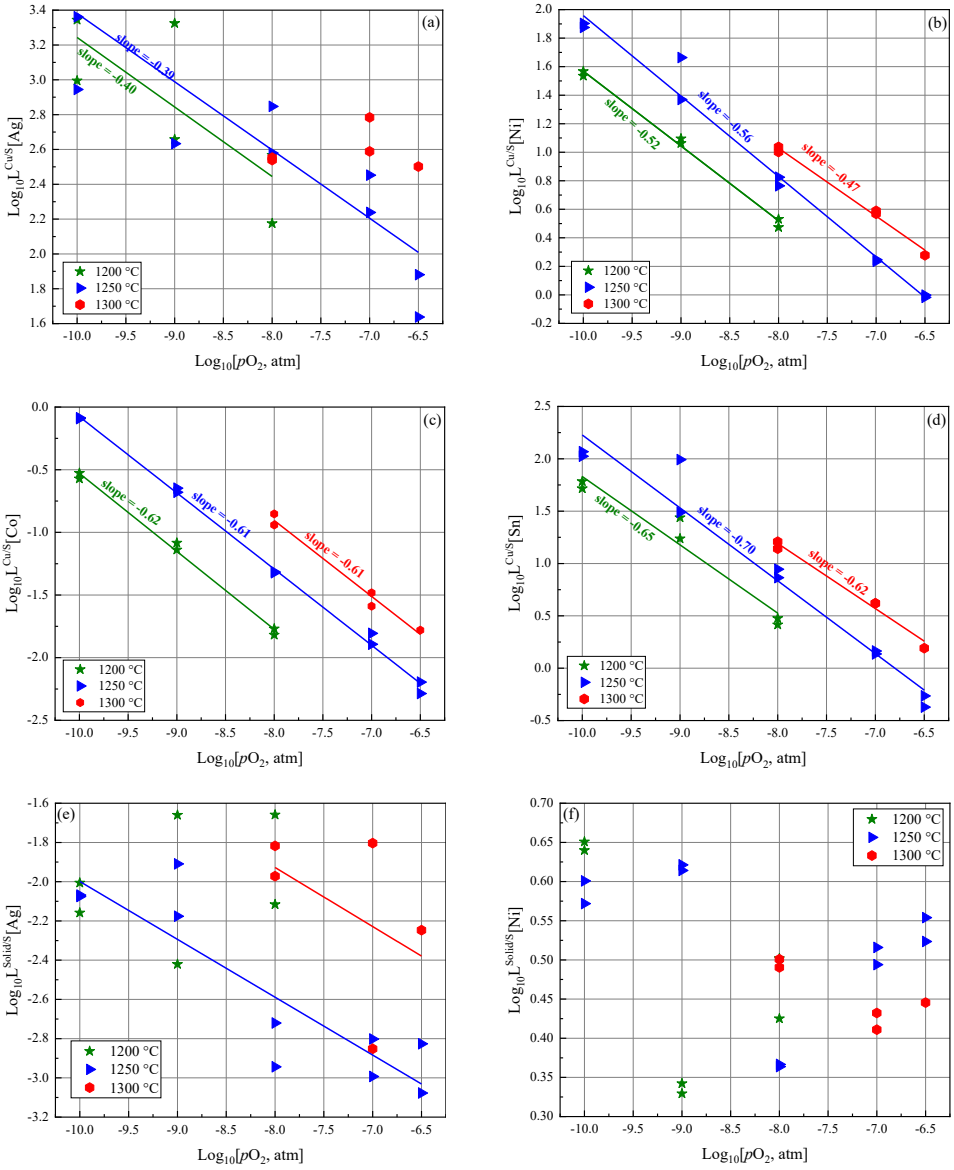

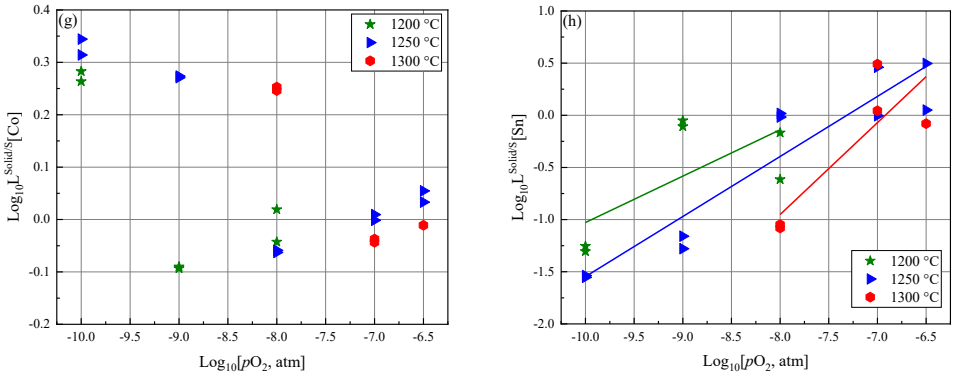

Figure 20. Logarithmic distribution coefficients of precious/high-tech metals between copper alloy/solids and slag at 1200-1300 °C: (a)-(d) logarithmic distribution coefficients of precious/high-tech metals between copper alloy and slag; (e)-(h) logarithmic distribution coefficients of precious/high-tech metals between spinel/wüstite and slag.

The logarithmic distribution coefficient of Ag between copper alloy and slag varied between 1.6 and 3.4 at 1200-1300 °C, indicating that Ag reported significantly to the copper alloy. The present distribution coefficient values for Ag at 1200-1250 °C decreased with increasing pO_2; however, the results determined at 1300 °C stayed almost constant, at around 2.6. The logarithmic distribution coefficient of Ag increased by approximately 0.2 log units with increasing temperature from 1200 °C to 1250 °C. The slopes of the trend lines at 1200 °C and 1250 °C in this study were -0.40 and -0.39, respectively, indicating that Ag oxide dissolves in the slag with a combination valence of 1+ and 2+, which is similar to the observations by Avarmaa et al. [29], since the species of $AgO_{0.5}$ and AgO would have slopes of -0.25 and -0.5, respectively.

The logarithmic distribution coefficients of Ni, Co, and Sn displayed similar decreasing trends with increasing pO_2. The distribution coefficient values for Ni and Sn were above zero, indicating that Ni and Sn preferred the copper alloy over the slag phase. However, Co displayed the opposite distribution tendency of accumulating in the slag phase. The slope of the trend lines for Ni at 1200-1300 °C was approximately -0.5, indicating that Ni dissolved into the slag as divalent oxide NiO, which is in good agreement with the observations in the literature [34, 118]. The slope of the trend lines for Co at 1200-1300 °C was around -0.60. This indicated that the cobalt in the slag existed as a combination of Co^{2+} and Co^{3+}, as reported by Takeda et al. [118], since the species CoO and Co_2O_3 would have slopes of -0.5 and -0.75, respectively. As for Sn, the slopes of the trend lines at 1200-1300 °C were from -0.6 to -0.7, which suggested that the tin in the slags had a mixed valence of 2+ and 4+ since the species SnO and SnO_2 would have slopes of -0.5 and -1, respectively.

Figure 20(e) indicates that Ag preferred the slag phase over the solid spinel/wüstite and the distribution coefficients at 1250-1300 °C displayed decreasing trends with increasing pO_2. The logarithmic distribution coefficient results at 1200 °C fluctuated around -2. The increase in temperature from 1250 °C to 1300 °C resulted in an increase in the distribution coefficient of Ag between solids and slag by approximately 0.6 log units. Ni was distributed two to four times more in the solid spinel/wüstite phase than in the molten slag. The distribution coefficient of Ni between spinel/wüstite and slag at all temperatures investigated decreased first and then increased with increasing pO_2. Co displayed similar trends as Ni; however, Co was distributed more into the slag phase at a given pO_2 and the increase of temperature favored the transfer of Co to the slag over the solid spinel/wüstite phases.

The negative slope of the trend line for the logarithmic distribution coefficient of Ag between solid spinel/wüstite and slag suggested that Ag reduced to a lower valence state in spinel/wüstite from the molten slag, independently of the slag saturation phase. In contrast, Sn was oxidized to higher valence states from the molten slag phase to spinel/wüstite, i.e., predominantly divalent in wüstite (FeO) and tetravalent in spinel (Fe_3O_4). Both Ni and Co in the solid phases were reduced to lower valent oxide species (MeO) from the molten slag when the slag was saturated with wüstite. However, they were oxidized further to higher valent species when the slag was saturated with spinel. A higher temperature favored the transfer of Ni and Co to wüstite but depressed their distribution into spinel.

4.3 Matte-slag-spinel-gas equilibrium system

Nowadays, the production of copper slag is increasing dramatically, due to the increased productivity of copper smelters as well as the depletion of primary copper ores. Currently, copper slag is mainly disposed of in landfills which occupy plenty of land and pose big threats to the environment and biodiversity due to the release of hazardous elements into the soil and groundwater. By lowering the silica concentration in the slag, i.e., adjusting the slag saturation to spinel saturation, the increasing slag-to-metal ratio of about 3 (w/w) in copper smelting can be effectively reduced.

4.3.1 Phase equilibria of matte and spinel-saturated iron silicate slag

The phase equilibria of matte and Fe-spinel-saturated iron silicate slags (FeO_x-SiO_2, FeO_x-SiO_2-Al_2O_3, and FeO_x-SiO_2-CaO) were investigated at 1250 °C and a pSO_2 of 0.25 atm. The typical microstructure of the matte-slag system in equilibrium with spinel is shown in Figure 21. Copper-rich veins were observed in matte, similar to the observations made for silica saturation. Both primary and secondary spinel crystals were found in the slag phase. The copper-rich veins in the matte and the secondary spinel crystals were formed during quenching.

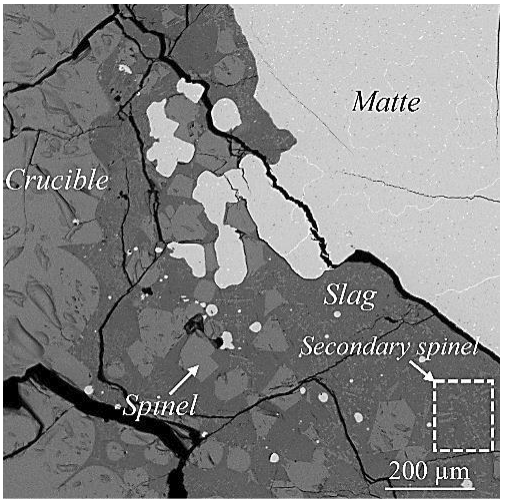

Figure 21. Typical microstructures of the matte-slag-spinel equilibrium system obtained at 1250 °C and pSO_2 of 0.25 atm.

Figure 22 shows the equilibrium compositions of matte, slag, and spinel as a function of oxygen partial pressure or matte grade. The copper concentration in the matte equilibrated with all types of slags increased with an increase in the prevailing oxygen partial pressure. Similar increasing trends have also been reported in the literature [94-101] due to the stronger oxidation of iron into the slag phase at higher pO_2, but the influence of oxygen partial pressure on the matte grade gradually decreased at higher pO_2. The addition of Al_2O_3 into spinel-saturated iron silicate slag led to an increase of copper concentration in the matte at a fixed pO_2, whereas the effect of CaO on the matte grade was not evident. Similarly to the results obtained for silica saturation, the concentrations of iron, sulfur, and oxygen in the matte displayed linear decreasing trends with increasing matte grade, as observed in previous studies [94-101], independent of the corresponding equilibrated type of slag. Compared with iron and sulfur, the concentration of oxygen in the matte was much lower, decreasing from approximately 2.0 wt% to 0.5 wt%.

The copper concentration in spinel-saturated iron silicate slag decreased from approximately 2.5 wt% to 0.5 wt% over the matte grade range of 60-70 wt% Cu, after which it started to increase at higher matte grades. Similar trends have also been observed by Hidayat et al. [95, 96]. Additions of Al_2O_3 or CaO to spinel-saturated iron silicate slag resulted in a decrease of copper concentration in the slag at matte grades lower than 70 wt% Cu. The concentrations of sulfur in the slag displayed decreasing trends with increasing matte grade, as reported in the literature [94-101]. Additions of Al_2O_3 and CaO into spinel-saturated iron silicate slag had decreasing impacts on the sulfur concentration in the slag. The concentrations of "FeO" and SiO_2 in all the spinel-saturated iron silicate slags displayed decreasing and increasing trends with increasing matte grade, respectively. Subsequently, the Fe/SiO_2 ratio in the present spinel-saturated iron silicate slag decreased over the entire matte grade range studied. The concentrations of Al_2O_3 and CaO in the slag increased from approximately 2.5-4 wt% and 4-7 wt%, respectively, with increasing matte grade, whereas the concentration of Al_2O_3 in the slag was approximately 3 wt% lower than that of CaO due to its dissolution in the spinel phase, as shown in Figure 22(k). The slag modifiers had a significant influence on the "FeO", SiO_2, and Fe/SiO_2 in the slags. The logarithmic distribution coefficient of Al_2O_3 between spinel and slag indicates its preference to be distributed into the spinel phase over the molten slag and its transfer to the spinel was favored by decreasing the prevailing oxygen partial pressure.

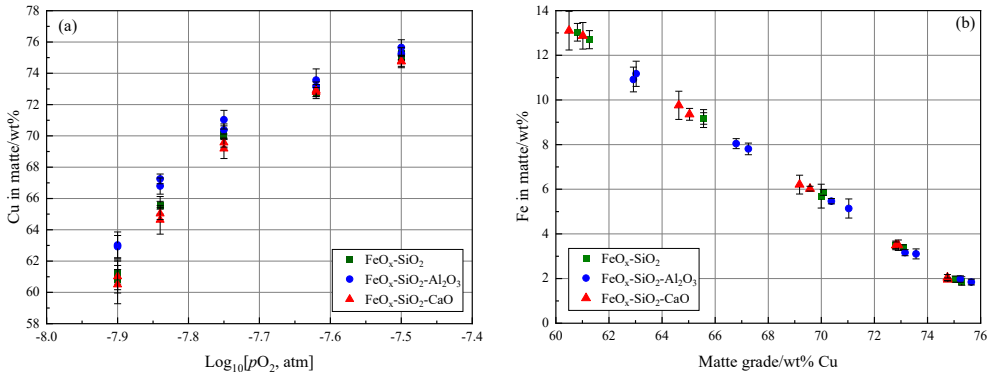

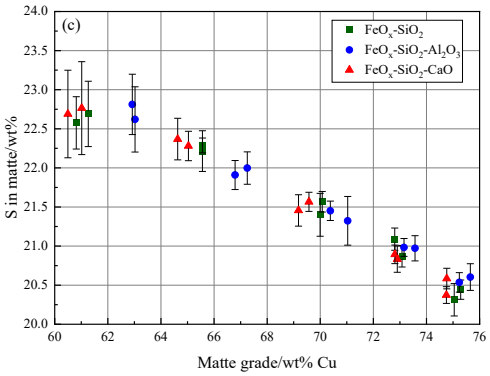
(c)
FeOx-SiO2
FeOx-SiO2-Al2O3
FeOx-SiO2-CaO
S in matte/wt%
Matte grade/wt% Cu

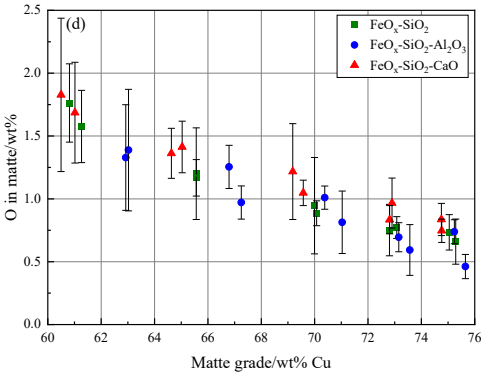
(d)
FeOx-SiO2
FeOx-SiO2-Al2O3
FeOx-SiO2-CaO
O in matte/wt%
Matte grade/wt% Cu

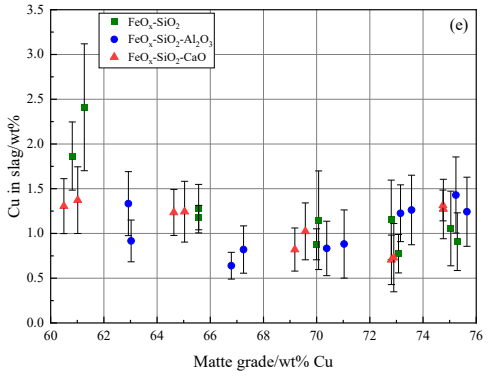
(e)
FeOx-SiO2
FeOx-SiO2-Al2O3
FeOx-SiO2-CaO
Cu in slag/wt%
Matte grade/wt% Cu

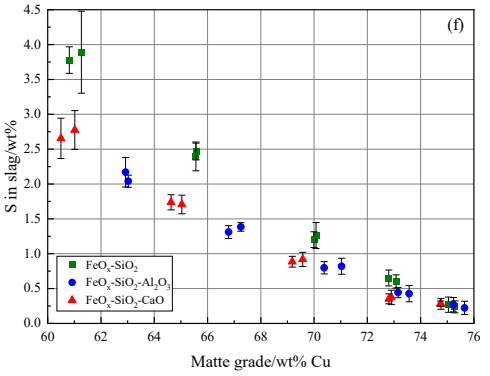
(f)
FeOx-SiO2
FeOx-SiO2-Al2O3
FeOx-SiO2-CaO
S in slag/wt%
Matte grade/wt% Cu

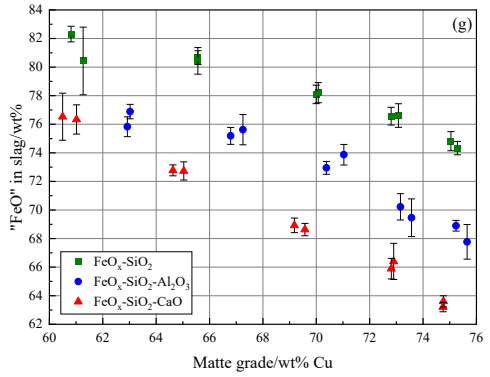
(g)
FeOx-SiO2
FeOx-SiO2-Al2O3
FeOx-SiO2-CaO
"FeO" in slag/wt%
Matte grade/wt% Cu

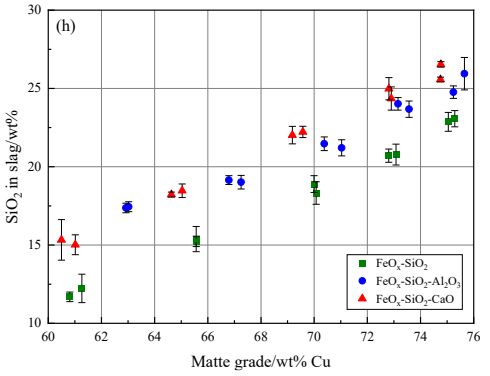
(h)
FeOx-SiO2
FeOx-SiO2-Al2O3
FeOx-SiO2-CaO
SiO2 in slag/wt%
Matte grade/wt% Cu

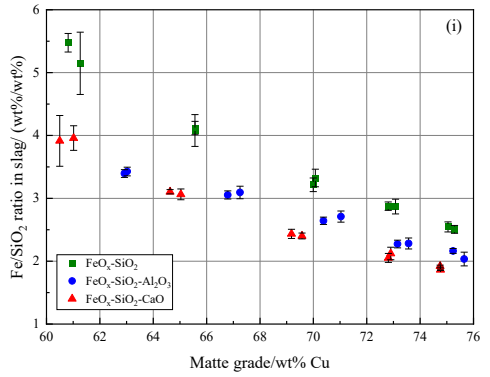
(i)
FeOx-SiO2
FeOx-SiO2-Al2O3
FeOx-SiO2-CaO
Fe/SiO2 ratio in slag/ (wt%/wt%)
Matte grade/wt% Cu

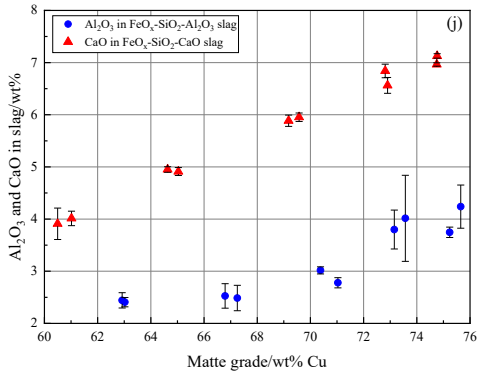
(j)
Al2O3 in FeOx-SiO2-Al2O3 slag
CaO in FeOx-SiO2-CaO slag
Al2O3 and CaO in slag/wt%
Matte grade/wt% Cu

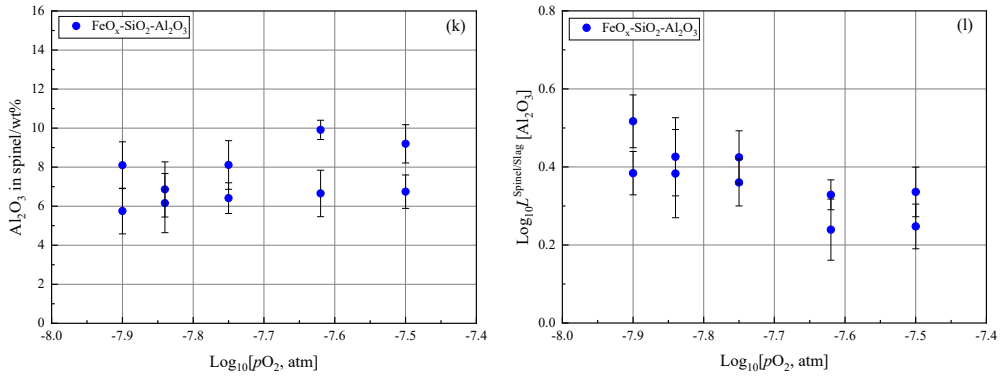

Figure 22. Equilibrium compositions of matte, slag, and spinel as a function of matte grade or oxygen partial pressure at 1250 °C and pSO2 of 0.25 atm: (a)-(d) matte composition; (e)-(i) slag composition; (j)-(k) spinel composition.

4.3.2 Precious/high-tech metal distributions between matte and spinel-saturated iron silicate slag

The distributions of the precious/high-tech metals Ag, Ni, Co, and Sn between the copper matte and spinel-saturated iron silicate slag were investigated over the matte grade range of 60-76 wt% Cu at 1300 °C and a pSO_2 of 0.25 atm. The concentrations of the metals in the matte, slag, and spinel phases are shown in Figure 23.

Figure 23(a) indicates that Ag displayed the highest concentration in the matte when compared with the high-tech metals investigated in this study, fluctuating around 1 wt%. It was found that the slag modifiers Al_2O_3 and CaO had no impact on the concentrations of Ag, Ni, and Co in the matte, as shown in Figures 23(a)-(c). The Ni concentration in the matte remained almost constant at 0.8 wt% within the matte grade range of 60-70 wt% Cu, after which it started to decrease with increasing matte grade. The concentration of Co in the matte decreased from approximately 0.2 to 0.05 wt% with increasing matte grade. Sn exhibited the lowest concentration in the matte, varying between 2 and 8 ppmw, as shown in Figure 23(d). Unlike Ag, Ni, and Co, the addition of CaO into the spinel-saturated iron silicate slag resulted in a small increase of Sn concentration in the matte; however, the effect of Al_2O_3 was not evident.

The concentration of Ag in the slags shown in Figure 23(e) decreased with increasing matte grade from 60 wt% Cu to approximately 70 wt% Cu, after which it started to increase at higher matte grades. The effects of the slag modifiers Al_2O_3 and CaO on this particular spinel-saturated iron silicate slag were not evident. The Ni concentration in the spinel-saturated iron silicate slags fluctuated around 0.06 wt% over the matte grade range of 60-70 wt% Cu and then displayed an increasing trend with increasing matte grade, regardless of the slag modifiers. The concentration of Co in all the slags exhibited slightly increasing trends with increasing matte grade. The slag modifiers Al_2O_3 and CaO had minor decreasing impacts on the Co concentration in the spinel-saturated slags. The concentration of Sn in the spinel-saturated FeO_x-SiO_2 slag displayed an increasing trend with increasing matte grade. However, the concentration of Sn in this particular Al_2O_3/CaO-containing slag remained almost constant at 10 ppmw when the matte grade was lower than 70 wt% Cu, after which it tended to increase with increasing matte grade.

The results for the dissolution of the precious/high-tech metals in spinel, as shown in Figures 23(i)-(l), suggest that varying concentrations of the metals dissolved into the spinel phase. The concentration of Ag in the spinel was extremely low (< 1 ppmw) and showed significant changes against the matte grade, similar to the results obtained from the Fe-spinel in equilibrium with metallic copper and slag. The results for Ni and Co in the spinel displayed a similar increasing trend with increasing matte grade, although the Co concentration in the spinel was approximately 0.05 wt% higher than that of Ni over the matte grade range of 62-70 wt% Cu. The concentration of Sn in the spinel varied between zero and approximately 300 ppmw without a clear trend and with a large standard deviation when compared to the other metals in the system investigated.

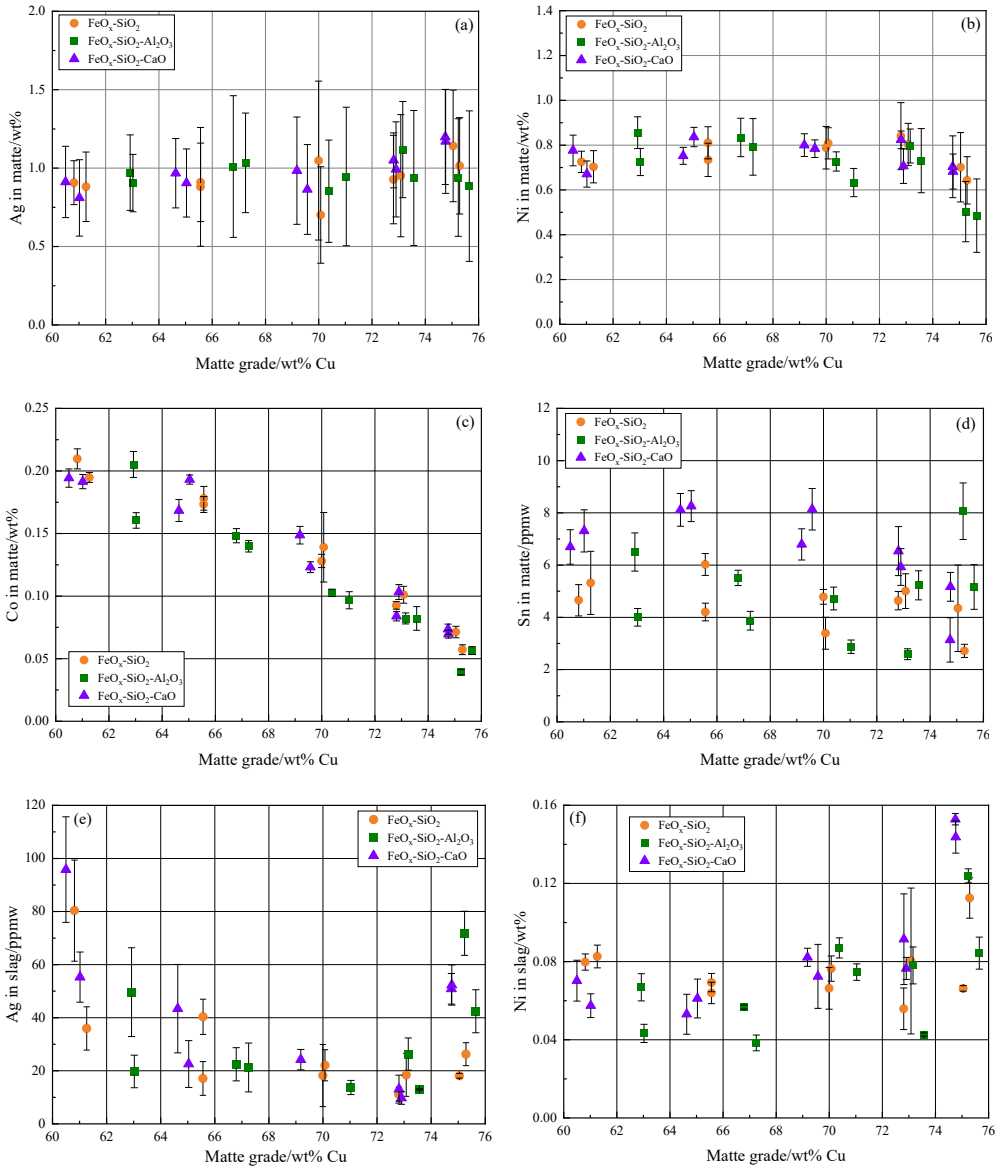

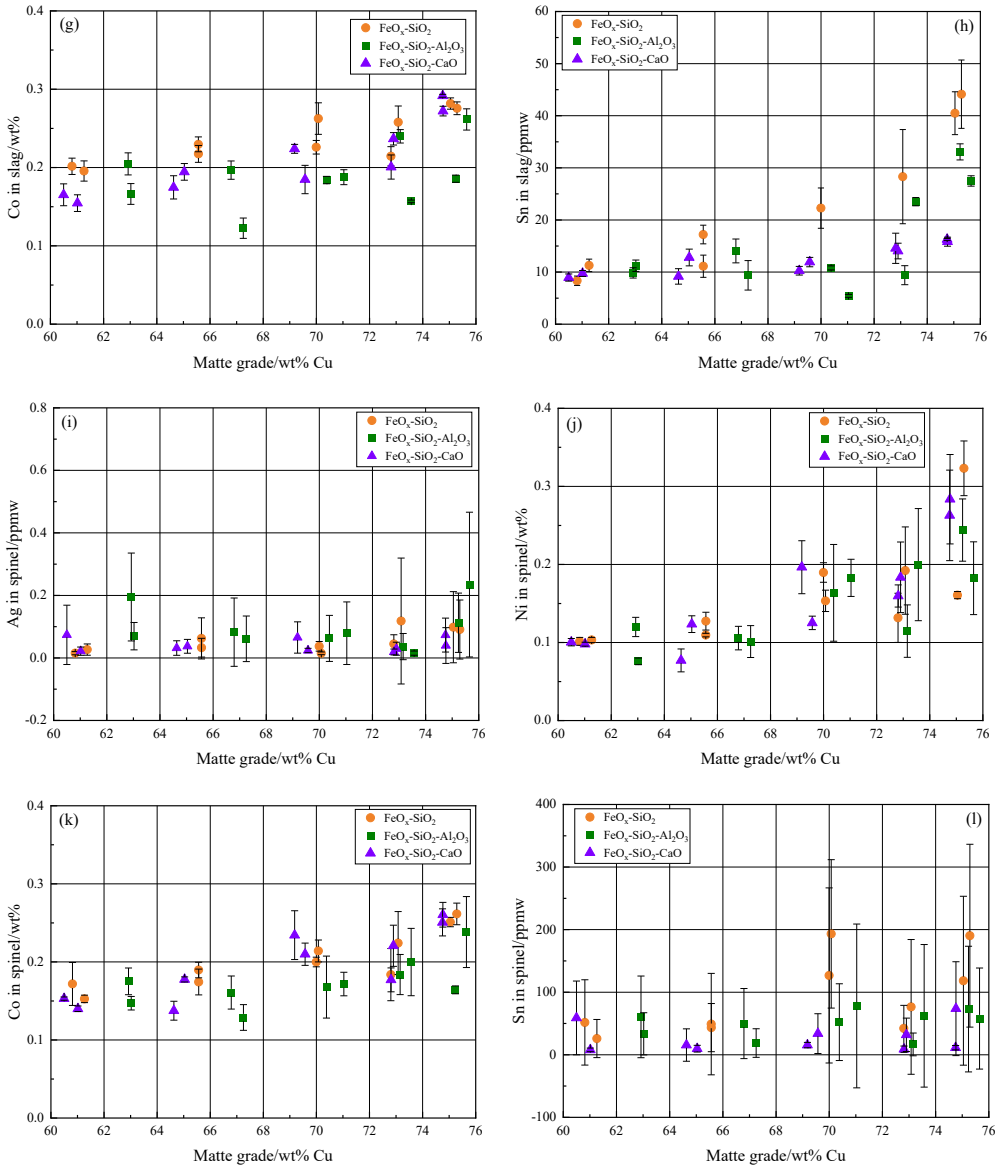

Figure 23. Concentrations of the precious/high-tech metals in matte, slag, and spinel as a function of matte grade at 1250 °C and pSO_2 of 0.25 atm: (a)-(d) precious/high-tech metals in matte; (e)-(h) precious/high-tech metals in slag; (i)-(l) precious/high-tech metals in spinel.

The logarithmic distribution coefficients of the precious/high-tech metals between matte/spinel and slag at 1250 °C and a pSO_2 of 0.25 atm are shown in Figure 24. The distribution results for Ag shown in Figure 24(a) indicate that Ag significantly favored the matte phase over the slag and the transfer of Ag to the matte can be improved by increasing the matte grade, as also reported by Roghani et al. [92] at magnesia saturation. The distribution of Ag between matte and spinel-saturated iron silicate slag was not affected by slag modifiers, which differs from the observations obtained at silica saturation in slags [92, 93]. Similarly to Ag, Ni preferred the matte phase over the slag in the entire matte grade range studied. The distribution

coefficients of Ni between the matte and spinel-saturated iron silicate slag displayed a slightly increasing trend over the matte grade range from 60 wt% Cu to approximately 66 wt% Cu, after which it started to decrease at higher matte grades. The logarithmic distribution coefficients of Co and Sn between matte and spinel-saturated slag displayed similar decreasing trends with increasing matte grade. The distribution results for Co and Sn were below zero, indicating that both Co and Sn preferentially distributed into slag over matte, as reported by Sukhomlinov et al. [35].

The logarithmic distribution coefficients of precious/high-tech metals between spinel and slag, as shown in Figures 24(e)-(h), give a better understanding of the distribution mechanism of trace metals in matte-slag-spinel equilibrium systems. Figure 24(e) indicates that Ag favored the molten slag more than the spinel and that the distribution coefficient increased with increasing matte grade. The slag modifiers Al_2O_3 and CaO into the spinel-saturated iron silicate slag studied had no evident impact on the distribution of Ag between spinel and slag, similarly to nickel, cobalt, and tin. The spinel-slag distribution coefficients for Ni and Sn indicated their preference for spinel over molten slag. The results for Ni exhibited an increasing trend with increasing matte grade, whereas the logarithmic distribution coefficient of Sn between spinel and slag remained at almost 0.5 over the whole matte grade range investigated. Co was slightly enriched in the molten slag as a function of matte grade, and the distribution results for Co showed no significant changes over the matte grade.

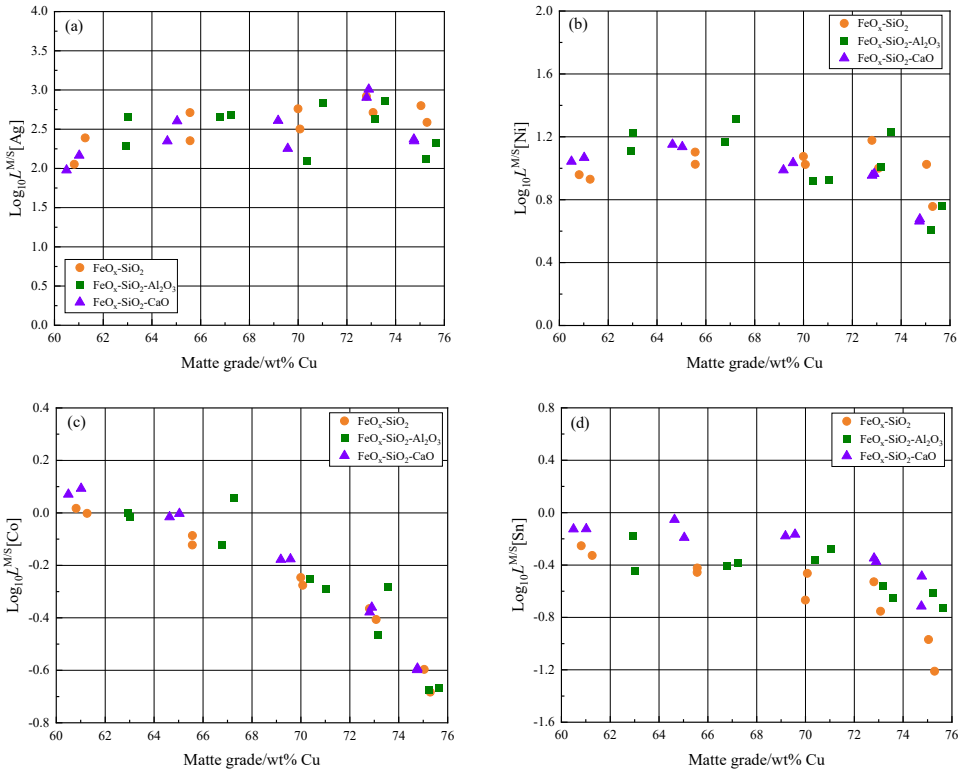

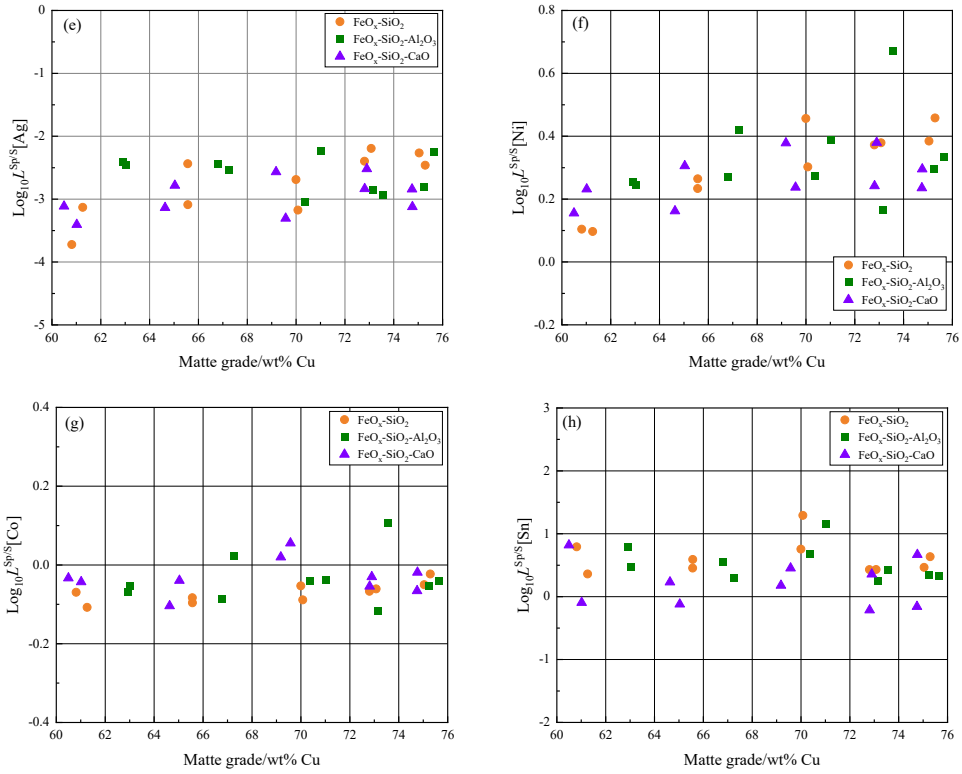

Figure 24. Logarithmic distribution coefficients of precious/high-tech metals between matte/spinel and slag at 1250 °C and pSO_2: (a)-(d) logarithmic distribution coefficients of precious/high-tech metals between matte and slag; (e)-(h) logarithmic distribution coefficients of precious/high-tech metals between spinel and slag.

5. Conclusions

The phase equilibria and distributions of precious/high-tech metals between copper/matte and slag/spinel/wüstite at different slag saturations were investigated using the high-temperature isothermal equilibration technique followed by drop quenching and direct phase composition analyses using EPMA and LA-ICP-MS. The experimental conditions were selected to simulate the primary and secondary copper smelting processes. The effects of slag modifiers (Al_2O_3 and CaO), pSO_2, saturation phase, and temperature on the phase equilibria of copper/matte and slag and on the precious/high-tech metals distributions in the equilibrium systems were studied. The direct phase analyses using EPMA and LA-ICP-MS eliminated potential uncertainties and errors in the phase assays due to the entrainment of another phase.

The phase equilibria and distributions of precious metals (Au, Ag, Pt, and Pd) between copper matte and silica-saturated FeO_x-SiO_2, FeO_x-SiO_2-Al_2O_3, and FeO_x-SiO_2-Al_2O_3-CaO slags were investigated at 1300 °C and a pSO_2 of 0.1-0.5 atm over a wide matte grade range from 55 wt% Cu to approximately 75 wt% Cu, which is related to the primary copper smelting process. The industrial secondary copper smelting/converting process was investigated by equilibrating the spinel/wüstite-saturated FeO_x-SiO_2 slag and metallic copper with precious/high-tech metals (Ag, Ni, Co, and Sn) at 1200-1300 °C and a pO_2 of 10^{-10}-$10^{-6.5}$ atm. Moreover, a novel fluxing strategy for copper matte smelting and precious/high-tech metals recycling was studied by smelting copper matte with precious/high-tech metals and spinel-saturated FeO_x-SiO_2, FeO_x-SiO_2-Al_2O_3, and FeO_x-SiO_2-CaO slags at 1250 °C and a pSO_2 of 0.25 atm.

The results for the phase equilibria of matte and silica/spinel/wüstite-saturated iron silicate slag indicated that the copper concentration in matte was highly dependent on the oxygen partial pressure and was affected by both the prevailing sulfur dioxide partial pressure and the slag saturation. The concentrations of iron, sulfur, and oxygen in the matte decreased with increasing matte grade, irrespective of the pSO_2 and slag modifiers. The copper concentration in the silica-saturated slag decreased with decreasing matte grade and by adding Al_2O_3 and CaO, regardless of the pSO_2, whereas the sulfur concentration in the slag was not affected by the pSO_2 and slag fluxes. The comparison of the results obtained at silica and spinel saturation suggested that the copper concentration in the slag was affected by the primary phase present in the slag, i.e., the copper concentration in the spinel-saturated slag was higher than that in the silica-saturated slag at a given matte grade when the matte grade was lower than 70 wt% Cu. The copper concentration in the spinel/wüstite-saturated iron silicate slag in equilibrium with metallic copper increased with increasing pO_2 and decreasing temperature.

The distribution coefficient data suggested that the precious metals Au, Ag, Pt, and Pd can be effectively recovered into matte and metal through the primary and secondary copper smelting routes. The slag modifiers Al_2O_3 and CaO improved the transfer of precious metals to the

matte in equilibrium with silica-saturated iron silicate slag, whereas their effects on the transfer of Ag and other high-tech metals were not evident when the system was saturated with spinel. The distributions of precious metals were not strongly affected by the prevailing sulfur dioxide partial pressure, as shown in Table 7, indicating that oxygen enrichment has only a minor direct impact on the distribution coefficients of trace elements. Unlike the precious metals, the high-tech metals investigated in this study exhibited different distribution behavior in primary and secondary copper smelting. In general, Ni and Sn favored the matte and metal phases at lower matte grades or in reducing conditions. However, Co was mainly distributed into the slag phase. A higher temperature favored the transfer of Ni, Co, and Sn to metal in secondary copper smelting. Sn was found to evaporate significantly during smelting. A strong dissolution of Ni, Co into spinel was observed, especially at higher oxygen partial pressures.

Table 7. Concentrations of copper in the slag and distribution coefficients of precious metals between matte and FeO_x-SiO_2 slag at the reference point of 65 wt% Cu in matte.

System	Saturation	pSO_2/atm	Temperature/°C	Cu in slag/wt%	$Log_{10}L^{m/s}$			
					Au	Ag	Pt	Pd
Matte-slag	Silica	0.1	1300	1.0	3.2	2.1	3.4	3.4
	Silica	0.5	1300	1.0	3.2	2.2	3.5	3.3
	Spinel	0.25	1250	1.4	/	2.4	/	/

The results for the phase equilibria of the major components (metal, matte, slag, tridymite, and spinel/wüstite) and the equilibrium distributions of precious/high-tech metals are valuable for updating thermodynamic databases and can be further used for thermodynamic modeling. From the perspective of industrial practice, the present results provide guidance for improving the performance of copper smelters and the recoveries of valuable metals from secondary materials by adjusting the temperature, oxygen/fuel to air ratio, as well as by adding fluxes into the slags.

References

[1] Cui, J., Zhang, L. (2008). Metallurgical recovery of metals from electronic waste: A review. *Journal of Hazardous Materials*, 158(2-3), 228-256.

[2] Shuva, M. A. H., Rhamdhani, M. A., Brooks, G. A., Masood, S., Reuter, M. A. (2016). Thermodynamics data of valuable elements relevant to e-waste processing through primary and secondary copper production: a review. *Journal of Cleaner Production*, 131, 795-809.

[3] Kojo, I. V., Jokilaakso, A., Hanniala, P. (2000). Flash smelting and converting furnaces: a 50 year retrospect. *JOM*, 52(2), 57-61.

[4] Directive 2012/19/EU of the European Parliament and of the Council of 4 July 2012 on waste electrical and electronic equipment, WEEE. Official Journal of the European Union L, 197, 38-71. Available at: https://eur-lex.europa.eu/legal-content/EN/TXT/PDF/?uri=CELEX:32012L0019&from=EN.

[5] Messmann, L., Helbig, C., Thorenz, A., Tuma, A. (2019). Economic and environmental benefits of recovery networks for WEEE in Europe. *Journal of Cleaner Production*, 222, 655-668.

[6] Lehner, T. (1999). Integrated recycling of non-ferrous metals at Boliden Ltd., Rönnskär smelter. In: *Proceedings of IEEE International Symposium on Electronics and the Environment*, Oak Brook, IL, USA, pp. 42-47.

[7] Veldhuizen, H., Sippel, B. Mining discarded electronics. *Industry and Environment*., 17(3), (1994), pp. 7-11.

[8] Hagelüken, C. (2006). Recycling of electronic scrap at Umicore's integrated metals smelter and refinery. *Erzmetall*, 59(3), 152-161.

[9] Hagelüken, C., Corti, C. W. (2010). Recycling of gold from electronics: Cost-effective use through 'Design for Recycling'. *Gold Bulletin*, 43(3), 209-220.

[10] Lennartsson, A., Engström, F., Samuelsson, C., Björkman, B., Pettersson, J. (2018). Large-Scale WEEE recycling integrated in an ore-based Cu-extraction system. *Journal of Sustainable Metallurgy*, 4(2), 222-232.

[11] Flores G. R. A., Nikolic, S., Mackey, P. J. (2014). ISASMELT™ for the recycling of E-scrap and copper in the US case study example of a new compact recycling plant, *JOM*, 66(5), pp. 823-832.

[12] Brusselaers, J., Mark, F. E., Tange, L. (2006). Using metal-rich WEEE plastics as feedstock/fuel substitute for an integrated metals smelter. *PlasticsEurope*, Brussels, Belgium.

[13] Khaliq, A., Rhamdhani, M. A., Brooks, G., Masood, S. (2014). Metal extraction processes for electronic waste and existing industrial routes: a review and Australian perspective. *Resources*, 3(1), 152-179.

[14] Brusselaers, J., Mark, F. E., Tange L. (2006). Technical Report, Plastics Europe, Brussels, Belgium. Available at: https://www.isasmelt.com/en/download/TechnicalPapersIsasmelt/Using_metal-rich_WEEE_plastics_as_feed.pdf

[15] Wang, M., Tan, Q., Chiang, J. F., Li, J. (2017). Recovery of rare and precious metals from urban mines-A review. *Frontiers of Environmental Science & Engineering*, 11(5), 1-17.

[16] Zhang, L., Xu, Z. (2016). A review of current progress of recycling technologies for metals from waste electrical and electronic equipment. *Journal of Cleaner Production*, 127, 19-36.

[17] Cesaro, A., Marra, A., Kuchta, K., Belgıorno, V., Van Hullebusch, E. D. (2018). WEEE management in a circular economy perspective: An overview. *Glob. Nest J*, 20, 743-750.

[18] Zeng, X., Mathews, J. A., Li, J. (2018). Urban mining of e-waste is becoming more cost-effective than virgin mining. *Environmental Science & Technology*, 52(8), 4835-4841.

[19] Shuva, M. A. H., Rhamdhani, M. A., Brooks, G. A., Masood, S. H., Reuter, M. A. (2017). Thermodynamics of palladium (Pd) and tantalum (Ta) relevant to secondary copper smelting. *Metallurgical and Materials Transactions B*, 48(1), 317-327.

[20] Wood, J., Creedy, S., Matusewicz, R., Reuter, M. (2011). Secondary copper processing using Outotec Ausmelt TSL technology. *Proceedings of MetPlant*, 460-467.

[21] Anindya, A., Swinbourne, D. R., Reuter, M. A., Matusewicz, R. W. (2013). Distribution of elements between copper and FeO_x-CaO-SiO_2 slags during pyrometallurgical processing of WEEE: Part 1-Tin. *Mineral Processing and Extractive Metallurgy*, 122(3), 165-173.

[22] Akcil, A., Erust, C., Gahan, C. S., Ozgun, M., Sahin, M., Tuncuk, A. (2015). Precious metal recovery from waste printed circuit boards using cyanide and non-cyanide lixiviants-a review. *Waste Management*, 45, 258-271.

[23] Huang, K., Guo, J., Xu, Z. (2009). Recycling of waste printed circuit boards: A review of current technologies and treatment status in China. *Journal of Hazardous Materials*, 164(2-3), 399-408.

[24] Tesfaye, F., Lindberg, D., Hamuyuni, J., Taskinen, P., Hupa, L. (2017). Improving urban mining practices for optimal recovery of resources from e-waste. *Minerals Engineering*, 111, 209-221.

[25] Klemettinen, L., Avarmaa, K., O'Brien, H., Taskinen, P., Jokilaakso, A. (2019). Behavior of tin and antimony in secondary copper smelting process. *Minerals*, 9(1), 39.

[26] Klemettinen, L., Aromaa, R., Dańczak, A., O'Brien, H., Taskinen, P., Jokilaakso, A. (2020). Distribution kinetics of rare earth elements in copper smelting. *Sustainability*, 12(1), 208.

[27] Klemettinen, L., Avarmaa, K., Taskinen, P. (2017). Trace element distributions in black copper smelting. *World of Metallurgy-Erzmetall*, 70(5), 257-264.

[28] Avarmaa, K., Klemettinen, L., O'Brien, H., Taskinen, P. (2019). Urban mining of precious metals via oxidizing copper smelting. *Minerals Engineering*, 133, 95-102.

[29] Avarmaa, K., O'Brien, H., Klemettinen, L., Taskinen, P. (2020). Precious metal recoveries in secondary copper smelting with high-alumina slags. *Journal of Material Cycles and Waste Management*, 22(3), 642-655.

[30] Avarmaa, K. (2019). Thermodynamic properties of WEEE-based minor elements in copper smelting processes. PhD thesis. Aalto University.

[31] Avarmaa, K., Yliaho, S., Taskinen, P. (2018). Recoveries of rare elements Ga, Ge, In and Sn from waste electric and electronic equipment through secondary copper smelting. *Waste Management*, 71, 400-410.

[32] Dańczak, A., Klemettinen, L., Kurhila, M., Taskinen, P., Lindberg, D., Jokilaakso, A. (2020). Behavior of battery metals lithium, cobalt, manganese and lanthanum in black copper smelting. *Batteries*, 6(1), 16.

[33] Dańczak, A., Klemettinen, L., O'Brien, H., Taskinen, P., Lindberg, D., Jokilaakso, A. (2021). Slag chemistry and behavior of nickel and tin in black copper smelting with alumina and magnesia-containing slags. *Journal of Sustainable Metallurgy*, 7(1), 1-14.

[34] Sukhomlinov, D., Klemettinen, L., Avarmaa, K., O'Brien, H., Taskinen, P., Jokilaakso, A. (2019). Distribution of Ni, Co, precious, and platinum group metals in copper making process. *Metallurgical and Materials Transactions B*, 50(4), 1752-1765.

[35] Sukhomlinov, D., Klemettinen, L., O'Brien, H., Taskinen, P., Jokilaakso, A. (2019). Behavior of Ga, In, Sn, and Te in copper matte smelting. *Metallurgical and Materials Transactions B*, 50(6), 2723-2732.

[36] Wan, X., Kleemola, L., Klemettinen, L., O'Brien, H., Taskinen, P., Jokilaakso, A. (2021). On the kinetic behavior of recycling precious metals (Au, Ag, Pt, and Pd) through copper smelting process. *Journal of Sustainable Metallurgy*, 7(3), 920-931.

[37] Avarmaa, K., Johto, H., Taskinen, P. (2016). Distribution of precious metals (Ag, Au, Pd, Pt, and Rh) between copper matte and iron silicate slag. *Metallurgical and Materials Transactions B*, 47(1), 244-255.

[38] B. Ebin, M.I. Isik. (2016). Pyrometallurgical processes for the recovery of metals from WEEE. A. Chagnes, G. Cote, C. Ekberg, et al. (Eds.), *WEEE Recycling*, Elsevier, pp. 107-138.

[39] Henao, H. M., Pizarro, C., Font, J., Moyano, A., Hayes, P. C., Jak, E. (2010). Phase equilibria of "Cu_2O"-"FeO"-CaO-MgO-Al_2O_3 slags at PO_2 of $10^{-8.5}$ atm in equilibrium with metallic copper for a copper slag cleaning production. *Metallurgical and Materials Transactions B*, 41(6), 1186-1193.

[40] Schlesinger, M. E., Sole, K. C., Davenport W. G.: Extractive metallurgy of copper. 5th ed., Elsevier, Oxford, 2011.

[41] Sridhar, R., Toguri, J. M., Simeonov, S. (1997). Thermodynamic considerations in copper pyrometallurgy. *JOM*, 49(4), 48.

[42] Tavera, F. J., Davenport, W. G. (1979). Equilibrations of copper matte and fayalite slag under controlled partial pressures of SO_2. *Metallurgical Transactions B*, 10(2), 237-241.

[43] Li, H., Rankin, W. J. (1994). Thermodynamics and phase relations of the Fe-O-S-Si_2 (sat) system at 1200 °C and the effect of copper. *Metallurgical and Materials Transactions B*, 25(1), 79-89.

[44] Nagamori, M. (1974). Metal loss to slag: Part I. Sulfidic and oxidic dissolution of copper in fayalite slag from low grade matte. *Metallurgical and Materials Transactions B*, 5(3), 531-538.

[45] Shimpo, R., Goto, S., Ogawa, O., Asakura, I. (1986). A study on the equilibrium between copper matte and slag. *Canadian Metallurgical Quarterly*, 25(2), 113-121.

[46] Yazawa, A. (1974). Thermodynamic considerations of copper smelting. *Canadian Metallurgical Quarterly*, 13(3), 443-453.

[47] Kashima, M., Eguchi, M., Yazawa, A. (1978). Distribution of impurities between crude copper, white metal and silica-saturated slag. *Transactions of the Japan Institute of Metals*, 19(3), 152-158.

[48] Kho, T. S., Swinbourne, D. R., Lehner, T. (2006). Cobalt distribution during copper matte smelting. *Metallurgical and Materials Transactions B*, 37(2), 209-214.

[49] Louey, R., Swinbourne, D. R., Lehner, T. (1999). Silver and tin distribution between copper matte and fayalite slag. In: *AusIMM Proceedings*. The Australian Institute of Mining and Metallurgy, 31-36.

[50] Fallah-Mehrjardi, A., Hidayat, T., Hayes, P. C., Jak, E. (2017). Experimental investigation of gas/slag/matte/tridymite equilibria in the Cu-Fe-O-S-Si system in controlled atmospheres: Development of technique. *Metallurgical and Materials Transactions B*, *48*(6), 3002-3016.

[51] Fallah-Mehrjardi, A., Hidayat, T., Hayes, P. C., Jak, E. (2019). Experimental investigation of gas/slag/matte/tridymite equilibria in the Cu-Fe-O-S-Si system in controlled gas atmosphere at T = 1200 °C and $P(SO_2)$ = 0.1 atm. *International Journal of Materials Research*, 110(6), 489-495.

[52] Yamaguchi, K. (2018). Thermodynamic study of the equilibrium distribution of platinum group metals between slag and molten metals and slag and copper matte. In: *Extraction 2018*, Springer, Cham, pp. 797-804.

[53] Avarmaa, K., O'Brien, H., Johto, H., Taskinen, P. (2015). Equilibrium distribution of precious metals between slag and copper matte at 1250-1350 °C. *Journal of Sustainable Metallurgy*, 1(3), 216-228.

[54] Avarmaa, K., Taskinen, P., Klemettinen, L., O'Brien, H., Lindberg, D. (2021). Ni-Fe-Co alloy-magnesia-iron-silicate slag equilibria and the behavior of minor elements Cu and P in nickel slag cleaning. *Journal of Materials Research and Technology*, 15, 719-730.

[55] Avarmaa, K., Klemettinen, L., O'Brien, H., Taskinen, P., Jokilaakso, A. (2019). Critical metals Ga, Ge and In: Experimental evidence for smelter recovery improvements. *Minerals*, 9(6), 367.

[56] Avarmaa, K., Klemettinen, L., O'Brien, H., Jokilaakso, A., Lindberg, D., Taskinen, P. (2021). Solubility of palladium in alumina-iron silicate melts. *JOM*, 73(6), 1871-1877.

[57] Avarmaa, K., Strengell, D., Johto, H., Latostenmaa, P., O'Brien, H., Taskinen, P. (2022). Solubility of chromium in DON smelting. *Mineral Processing and Extractive Metallurgy Review*, 43(2), 201-208.

[58] Klemettinen, L., Avarmaa, K., Sukhomlinov, D., O'Brien, H., Taskinen, P., Jokilaakso, A. (2020). Recycling of tellurium via copper smelting processes. *SN Applied Sciences*, 2(3), 1-9.

[59] Klemettinen, L., Avarmaa, K., O'Brien, H., Jokilaakso, A., Taskinen, P. (2020). Control of platinum loss in WEEE smelting. *JOM*, 72(7), 2770-2777.

[60] Klemettinen, L. (2021). Behaviour of trace elements in copper smelting processes - LA-ICP-MS as a tool for sample characterisation. PhD thesis. Aalto University.

[61] Hellstén, N., Klemettinen, L., Sukhomlinov, D., O'Brien, H., Taskinen, P., Jokilaakso, A., Salminen, J. (2019). Slag cleaning equilibria in iron silicate slag-copper systems. *Journal of Sustainable Metallurgy*, 5(4), 463-473.

[62] Dańczak, A., Ruismäki, R., Rinne, T., Klemettinen, L., O'Brien, H., Taskinen, P., Jokilaakso, A., Serna-Guerrero, R. (2021). Worth from waste: utilizing a graphite-rich fraction from spent lithium-ion batteries as alternative reductant in nickel slag cleaning. *Minerals*, 11(7), 784.

[63] Sukhomlinov, D., Klemettinen, L., Virtanen, O., Lahaye, Y., Latostenmaa, P., Jokilaakso, A., Taskinen, P. (2020). Trace element distributions between matte and slag in direct nickel matte smelting. *Canadian Metallurgical Quarterly*, 59(1), 67-77.

[64] Holland, K., Sukhomlinov, D., Klemettinen, L., Latostenmaa, P., O'Brien, H., Jokilaakso, A., Taskinen, P. (2021). Distribution of Co, Fe, Ni, and precious metals between blister copper and white metal. *Mineral Processing and Extractive Metallurgy*, 130(4), 313-323.

[65] Wan, X. (2021). Experimental investigation on time-dependent recycling behaviour of WPCBs in copper flash smelting conditions. PhD thesis. Aalto University.

[66] Shishin, D., Hidayat, T., Sultana, U., Shevchenko, M., Jak, E. (2020). Experimental Study and Thermodynamic Calculations of the Distribution of Ag, Au, Bi, and Zn Between Pb Metal and Pb-Fe-O-Si slag. *Journal of Sustainable Metallurgy*, 6(1), 68-77.

[67] Shishin, D., Hidayat, T., Chen, J., Hayes, P. C., Jak, E. (2019). Experimental investigation and thermodynamic modeling of the distributions of Ag and Au between slag, matte, and metal in the Cu-Fe-O-S-Si system. *Journal of Sustainable Metallurgy*, 5(2), 240-249.

[68] Chen, J., Fallah-Mehrjardi, A., Specht, A., O'Neill, H. S. C. (2022). Measurement of minor element distributions in complex copper converting slags using quantitative microanalysis techniques. *JOM*, 74(1), 185-194.

[69] Davenport, W G., King, M., Schlesinger, M., Biswas, A. K. (2002). *Extractive Metallurgy of Copper* (4th ed.). Oxford, England: Pergamon Press. https://doi.org/10.1016/B978-0-08-044029-3.X5000-X ISBN 978-0-08-044029-3.

[70] Taskinen, P., Seppälä, K., Laulumaa, J., Poijärvi, J. (2001). Oxygen pressure in the Outokumpu flash smelting furnace - Part 1: Copper flash smelting settler. *Mineral Processing and Extractive Metallurgy*, 110(2), 94-100.

[71] Taskinen, P., Jokilaakso, A. (2021). Reaction sequences in flash smelting and converting furnaces: An in-depth view. *Metallurgical and Materials Transactions B*, *52*(5), 3524-3542.

[72] Guntoro, P. L., Jokilaakso, A., Hellsten, N., Taskinen, P. (2018). Copper matte-slag reaction sequences and separation processes in matte smelting. *Journal of Mining and Metallurgy B: Metallurgy*, 54(3), 301-311.

[73] Widmer, R., Oswald-Krapf, H., Sinha-Khetriwal, D., Schnellmann, M., Böni, H. (2005). Global perspectives on e-waste. *Environmental Impact Assessment Review*, 25(5), 436-458.

[74] Anindya, A., Swinbourne, D., Reuter, M., Matusewicz, R. (2009). Tin distribution during smelting of WEEE with copper scrap. In: *Proceedings of the European Metallurgical Conference EMC 2009*, Innsbruck, Austria, 28 June-1 July 2009; GDMB Verlag GmbH: Clausthal-Zellerfeld, Germany, 2009; pp. 555-568.

[75] Hughes, S., Jåfs, M., Johto, H., Stål, J., Karonen, J. (2019). Outotec solutions for e-scrap processing. In: *REWAS 2019*, Springer, Cham, pp. 283-294.

[76] Shuva, M. A. H., Rhamdhani, M. A., Brooks, G. A., Masood, S., Reuter, M. A., Firdaus, M. (2017). Analysis for optimum conditions for recovery of valuable metals from e-waste through black copper smelting. In: *8th International Symposium on High-Temperature Metallurgical Processing*. Springer, Cham, pp. 419-427

[77] Hagelüken, C. (2006). Recycling of electronic scrap at Umicore precious metals refining. *Acta Metallurgica Slovaca*, 12, 111-120.

[78] Brusselaers, J., Mark, F. E., Tange, L., 2006. Using metal-rich WEEE plastics as feedstock/fuel substitute for an integrated metals smelter. Technical report produced by PlasticsEurope in co-operation with Umicore and the European Flame Retardants Association. Available at: http://www.plasticseurope.org/

[79] Mulenshi, J. (2015). Mapping of settling processes at Boliden Rönnskär and Harjavalta Smelters. Master's thesis. Luleå University of Technology.

[80] Djordjevic, P., Mitevska, N., Mihajlovic, I., Nikolic, D., Zivkovic, Z. (2014). Effect of the slag basicity on the coefficient of distribution between copper matte and the slag for certain metals. *Mineral Processing and Extractive Metallurgy Review*, 35(3), 202-207.

[81] Nikolic, S., Hayes, P. C., Jak, E. (2009). Liquidus temperatures in the "Cu_2O"-FeO-Fe_2O_3-CaO-SiO_2 system at metallic copper saturation, at fixed oxygen partial pressures, and in equilibrium with spinel or dicalcium ferrite at 1200 °C and 1250 °C. *Metallurgical and Materials Transactions B*, 40(6):910-919.

[82] Abdeyazdan, H., Fallah-Mehrjardi, A., Hidayat, T., Shevchenko, M., Hayes, P. C., Jak, E. (2020). The effect of MgO on gas-slag-matte-tridymite equilibria in fayalite-based copper smelting slags at 1473 K (1200 °C) and 1573 K (1300 °C), and P(SO_2) = 0.25 atm. *Journal of Phase Equilibria and Diffusion*, 41(1), 44-55.

[83] Fallah-Mehrjardi, A., Hidayat, T., Hayes, P. C., Jak, E. (2018). Experimental investigation of gas/slag/matte/tridymite equilibria in the Cu-Fe-O-S-Si system in controlled gas atmosphere: experimental results at 1523 K (1250 °C) and P(SO_2) = 0.25 atm. *Metallurgical and Materials Transactions B*, 49(4), 1732-1739.

[84] Fallah-Mehrjardi, A., Hayes, P. C., Jak, E. (2018). The effect of CaO on gas/slag/matte/tridymite equilibria in fayalite-based copper smelting slags at 1473 K (1200 °C) and P(SO_2) = 0.25 atm. *Metallurgical and Materials Transactions B*, 49(2), 602-609.

[85] Fallah-Mehrjardi, A., Hidayat, T., Hayes, P. C., Jak, E. (2022). The influence of temperature and matte grade on gas-slag-matte-tridymite equilibria in the Cu-Fe-O-S-Si system at p(SO_2) = 0.25 atm. *Mineral Processing and Extractive Metallurgy*, 131(1), 53-60.

[86] Fallah-Mehrjardi, A., Hidayat, T., Hayes, P. C., Jak, E. (2022). The effect of sulfur dioxide partial pressure on gas-slag-matte-tridymite equilibria in the Cu-Fe-O-S-Si system at 1200 °C. *Mineral Processing and Extractive Metallurgy*, 131(1), 61-68.

[87] Shimpo, R., Goto, S., Ogawa, O., Asakura, I. (1986). A study on the equilibrium between copper matte and slag. *Canadian Metallurgical Quarterly*, 25(2), 113-121.

[88] Sineva, S., Fallah-Mehrjardi, A., Hidayat, T., Shevchenko, M., Shishin, D., Hayes, P. C., Jak, E. (2020). Experimental investigation of gas/slag/matte/tridymite equilibria in the Cu-Fe-O-S-Si-Al-Ca-Mg system in controlled gas atmosphere: experimental results at 1473 K (1200 °C), 1573 K (1300 °C) and p(SO_2) = 0.25 atm. *Journal of Phase Equilibria and Diffusion*, 41(3), 243-256.

[89] Hidayat, T., Jak, E., Fallah-Mehrjardi, A., Hayesa, P. C. (2020). The effect of Al_2O_3 on fayalite-based copper smelting slags in equilibrium with matte and tridymite at 1200 °C and P(SO_2) = 0.25 atm. *International Journal of Materials Research*, 111(4), 283-289.

[90] Takeda, Y. (1997). Copper solubility in matte smelting slag. In: *Molten Slags, Fluxes and Salts '97 Conference*: Sydney, Iron & Steel Society, Warrendale, PA, 329-339.

[91] Roghani, G., Hino, M., Itagaki, K. (1997). Phase equilibrium and minor element distribution between slag and copper matte under high partial pressures of SO_2. In: *Proceedings of the 5th International Conference on Molten Slags, Fluxes and Salts. Iron & Steel Society*, Warrendale, 693-703.

[92] Roghani, G., Hino, M., Itagaki, K. (1997). Phase equilibrium and minor elements distribution between SiO_2-CaO-FeO_x-MgO slag and copper matte at 1573 K under high partial pressures of SO_2. *Materials Transactions, JIM*, 38(8), 707-713.

[93] Roghani, G., Takeda, Y., Itagaki, K. (2000). Phase equilibrium and minor element distribution between FeOx-SiO_2-MgO-based slag and Cu_2S-FeS matte at 1573 K under high partial pressures of SO_2. *Metallurgical and Materials Transactions B*, 31(4), 705-712.

[94] Hidayat, T., Mehrjardi, A. F., Hayes, P. C., Jak, E. (2016). Experimental study of gas/slag/matte/spinel equilibria and minor elements partitioning in the Cu-Fe-O-S-Si system. In: *Advances in Molten Slags, Fluxes, and Salts: Proceedings of the 10th International Conference on Molten Slags, Fluxes and Salts 2016*, ed. R. G. Reddy, P. Chaubal, P. C. Pistorius, and U. Pal, 1207-1220. Cham: Springer.

[95] Hidayat, T., Fallah-Mehrjardi, A., Hayes, P. C., Jak, E. (2018). Experimental Investigation of Gas/slag/matte/spinel equilibria in the Cu-Fe-O-S-Si system at 1473 K (1200 °C) and $P(SO_2)$ = 0.25 atm. *Metallurgical and Materials Transactions B*, 49(4), 1750-1765.

[96] Hidayat, T., Fallah-Mehrjardi, A., Hayes, P. C., Jak, E. (2020). The influence of temperature on the gas/slag/matte/spinel equilibria in the Cu-Fe-O-S-Si system at fixed $P(SO_2)$ = 0.25 atm. *Metallurgical and Materials Transactions B*, 51(3), 963-972.

[97] Chen, M., Sun, Y., Balladares, E., Pizarro, C., Zhao, B. (2019). Experimental studies of liquid/spinel/matte/gas equilibria in the Si-Fe-O-Cu-S system at controlled $P(SO_2)$ 0.3 and 0.6 atm. *Calphad*, 66, 101642.

[98] Sun, Y., Chen, M., Balladares, E., Pizarro, C., Contreras, L., Zhao, B. (2020). Effect of CaO on the liquid/spinel/matte/gas equilibria in the Si-Fe-O-Cu-S system at controlled $P(SO_2)$ 0.3 and 0.6 atm. *Calphad*, 69, 101751.

[99] Sun, Y., Chen, M., Balladares, E., Pizarro, C., Contreras, L., Zhao, B. (2020). Effect of MgO on the liquid/spinel/matte/gas equilibria in the Si-Fe-Mg-O-Cu-S system at controlled $P(SO_2)$ 0.3 and 0.6 atm. *Calphad*, 70, 101803.

[100] Sineva, S., Fallah-Mehrjardi, A., Hidayat, T., Hayes, P. C., Jak, E. (2020). Experimental study of the individual effects of Al_2O_3, CaO and MgO on gas/slag/matte/spinel equilibria in Cu-Fe-O-S-Si-Al-Ca-Mg system at 1473 K (1200 °C) and $p(SO_2)$ = 0.25 atm. *Journal of Phase Equilibria and Diffusion*, 41(6), 859-869.

[101] Sineva, S., Hidayat, T., Fallah-Mehrjardi, A., Starykh, R., Hayes, P. C., Jak, E. (2021). Experimental investigation of gas-matte-spinel and gas-slag-matte-spinel equilibria in the Cu-Fe-O-S-Si system at 1200 °C: effect of SO_2 partial pressure. *Mineral Processing and Extractive Metallurgy*, 1-8.

[102] Ilyushechkin, A., Hayes, P. C., Jak, E. (2004). Liquidus temperatures in calcium ferrite slags in equilibrium with molten copper. *Metallurgical* and *Materials Transactions B*, 35(2), 203-215.

[103] Nikolic, S., Hayes, P. C., Jak, E. (2008). Phase equilibria in ferrous calcium silicate slags: Part III. Copper-saturated slag at 1250 °C and 1300 °C at an oxygen partial pressure of 10^{-6} atm. *Metallurgical and Materials Transactions B*, 39(2), 200-209.

[104] Nikolic, S., Hayes, P. C., Jak, E. (2008). Phase equilibria in ferrous calcium silicate slags: part IV. Liquidus temperatures and solubility of copper in "Cu_2O"-FeO-Fe_2O_3-CaO-SiO_2 slags at 1250 °C and 1300 °C at an oxygen partial pressure of 10^{-6} atm. *Metallurgical and Materials Transactions B*, 39(2), 210-217.

[105] Nikolic, S., Hayes, P. C., Jak, E. (2009). Experimental techniques for investigating calcium ferrite slags at metallic copper saturation and application to the systems "Cu_2O"-"Fe_2O_3" and "Cu_2O"-CaO at metallic copper saturation. *Metallurgical and Materials Transactions B*, 40(6), 892-899.

[106] Hidayat, T., Henao, H. M., Hayes, P. C., Jak, E. (2012). Phase equilibria studies of the Cu-Fe-O-Si system in equilibrium with air and with metallic copper. *Metallurgical and Materials Transactions B*, 43(5), 1034-1045.

[107] Hidayat, T., Henao, H. M., Hayes, P. C., Jak, E. (2012). Phase equilibria studies of Cu-O-Si systems in equilibrium with air and metallic copper and Cu-Me-O-Si systems (Me = Ca, Mg, Al, and Fe) in equilibrium with metallic copper. *Metallurgical and Materials Transactions B*, 43(6), 1290-1299.

[108] Hidayat, T., Hayes, P. C., Jak, E. (2018). Phase equilibria in the ZnO-"FeO"-SiO_2 system in reducing atmosphere and in the ZnO-"FeO"-SiO_2-"Cu_2O" system in equilibrium with liquid copper metal at 1250 °C (1523 K). *Metallurgical and Materials Transactions B*, 49(4), 1766-1780.

[109] Shishin, D., Shevchenko, M., Jak, E. (2021). Experimental study and thermodynamic calculations in the CaO-Cu_2O-FeO-Fe_2O_3-SiO_2 system for applications in novel copper-based processes. *Journal of Sustainable Metallurgy*, 7(1), 300-313.

[110] Klemettinen, L., Avarmaa, K., Taskinen, P. (2017). Slag chemistry of high-alumina iron silicate slags at 1300 °C in WEEE smelting. *Journal of Sustainable Metallurgy*, 3(4), 772-781.

[111] Wan, X., Shen, L., Jokilaakso, A., Eriç, H., Taskinen, P. (2021). Experimental approach to matte-slag reactions in the Flash Smelting Process. *Mineral Processing and Extractive Metallurgy Review*, 42(4), 231-241.

[112] Wang, Q. M., Wang, S. S., Tian, M., Tang, D. X., Tian, Q. H., Guo, X. Y. (2019). Relationship between copper content of slag and matte in the SKS copper smelting process. *International Journal of Minerals, Metallurgy, and Materials*, 26(3), 301-308.

[113] Sun, Y., Chen, M., Cui, Z., Contreras, L., Zhao, B. (2020). Phase equilibria of ferrous-calcium silicate slags in the liquid/spinel/white metal/gas system for the copper converting process. *Metallurgical and Materials Transactions B*, 51(5), 2012-2020.

[114] Taskinen, P., Avarmaa, K. (2021). Simulation of slag-matte/metal equilibria for complex and low-grade raw materials. *Sustainability*, 13(22), 12826.

[115] Taskinen, P. (2017). Industrial use of thermodynamic simulations in pyrometallurgy. In: *AIP Conference Proceedings* (Vol. 1805, No. 1, p. 020001). AIP Publishing LLC.

[116] Taskinen, P. (2011). Direct-to-blister smelting of copper concentrates: the slag fluxing chemistry. *Mineral Processing and Extractive Metallurgy*, 120(4), 240-246.

[117] Kojo, I., Storch, H. (2006). Copper production with Outokumpu flash smelting: an update. In: *Sohn international symposium*. Kongoli F., eds. Vol. 8. Warrendale (PA): TMS. pp. 225-238.

[118] Takeda, Y., Ishiwata, S., Yazawa, A. (1983). Distribution equilibria of minor elements between liquid copper and calcium ferrite slag. *Transactions of the Japan Institute of Metals*, 24 (7), 518-528.

[119] Roine, A. (2017) HSC Chemistry for Windows, v. 9.4.1 (Pori, Finland: Outotec Research, 2017). Available at: https://www.hsc-chemistry.com/news&tiedoteid=31

[120] Gisby, J., Taskinen, P., Pihlasalo, J., Li, Z., Tyrer, M., Pearce, J., Avarmaa, K., Björklund, P., Davies, H., Korpi, M., Martin, S., Pesonen, L., Robinson, J. (2017). MTDATA and the prediction of phase equilibria in oxide systems: 30 years of industrial collaboration. *Metallurgical and Materials Transactions B*, 48(1), 91-98.

[121] Davies, R.H., Dinsdale, A.T., Gisby, J.A., Robinson, J.A.J., Martin, A.M. (2002). MTDATA-thermodynamic and phase equilibrium software from the national physical laboratory. *Calphad*, 26(2), 229-271.

[122] Pouchou, J. L., Pichoir, F. (1986). Basic expression of "PAP" computation for quantitative EPMA. In: *11th International Congress on X-ray Optics and Microanalysis (ICXOM)*, (J. D. Brown and R. H. Packwood, Eds.), Ontario, Canada: Publ. Univ. Western Ontario, pp. 249-256.

[123] Van Achterbergh, E., Ryan, C. G., Jackson, S.E., Griffin, W. L. (2001). Data reduction software for LA-ICP-MS: Appendix. P.J. Sylvester (Ed.), Laser Ablation-ICP-Mass Spectrometry in the Earth Sciences: Principles and Applications, Mineralog. Assoc. Canada (MAC) Short Course Series, Ottawa, Ontario, Canada, vol. 29, 239-243.

Aalto-DT 146/2022

ISBN 978-952-64-0973-3 (printed)
ISBN 978-952-64-0974-0 (pdf)
ISSN 1799-4934 (printed)
ISSN 1799-4942 (pdf)

Aalto University
School of Chemical Engineering
Department of Chemical and Metallurgical Engineering
www.aalto.fi

BUSINESS + ECONOMY

ART + DESIGN + ARCHITECTURE

SCIENCE + TECHNOLOGY

CROSSOVER

DOCTORAL THESES